



**HAL**  
open science

## TTC12 loss-of-function mutations cause primary Ciliary Dyskinesia and unveil distinct dynein assembly mechanisms in motile cilia versus flagella

Lucie Thomas, Khaled Bouhouche, Marjorie Whitfield, Guillaume Thouvenin, Andre Coste, Bruno Louis, Claire Szymanski, Emilie Bequignon, Jean-François Papon, Manon Castelli, et al.

### ► To cite this version:

Lucie Thomas, Khaled Bouhouche, Marjorie Whitfield, Guillaume Thouvenin, Andre Coste, et al.. TTC12 loss-of-function mutations cause primary Ciliary Dyskinesia and unveil distinct dynein assembly mechanisms in motile cilia versus flagella. American Journal of Human Genetics, 2020, 106 (2), pp.153-169. 10.1016/j.ajhg.2019.12.010 . hal-02456263

**HAL Id: hal-02456263**

**<https://hal.science/hal-02456263v1>**

Submitted on 7 Mar 2022

**HAL** is a multi-disciplinary open access archive for the deposit and dissemination of scientific research documents, whether they are published or not. The documents may come from teaching and research institutions in France or abroad, or from public or private research centers.

L'archive ouverte pluridisciplinaire **HAL**, est destinée au dépôt et à la diffusion de documents scientifiques de niveau recherche, publiés ou non, émanant des établissements d'enseignement et de recherche français ou étrangers, des laboratoires publics ou privés.



Distributed under a Creative Commons Attribution - NonCommercial 4.0 International License

1 **TTC12 loss-of-function mutations cause primary ciliary dyskinesia and unveil distinct dynein**  
2 **assembly mechanisms in motile cilia versus flagella**

3 Lucie Thomas<sup>1</sup>, Khaled Bouhouche<sup>2,19</sup>, Marjorie Whitfield<sup>3,19</sup>, Guillaume Thouvenin<sup>4,5</sup>, Andre Coste<sup>6,7</sup>,  
4 Bruno Louis<sup>7</sup>, Claire Szymanski<sup>8</sup>, Emilie Bequignon<sup>6,7</sup>, Jean-François Papon<sup>7,9</sup>, Manon Castelli<sup>2</sup>, Michel  
5 Lemullois<sup>2</sup>, Xavier Dhalluin<sup>10</sup>, Valérie Drouin-Garraud<sup>11</sup>, Guy Montantin<sup>12</sup>, Sylvie Tissier<sup>12</sup>, Philippe  
6 Duquesnoy<sup>1</sup>, Bruno Copin<sup>12</sup>, Florence Dastot<sup>12</sup>, Sandrine Couvet<sup>1</sup>, Anne-Laure Barbotin<sup>13,14</sup>, Catherine  
7 Faucon<sup>15</sup>, Isabelle Honore<sup>16</sup>, Bernard Maitre<sup>17</sup>, Nicole Beydon<sup>4</sup>, Aline Tamalet<sup>4</sup>, Nathalie Rives<sup>18</sup>, France  
8 Koll<sup>2</sup>, Estelle Escudier<sup>1,12</sup>, Anne-Marie Tassin<sup>2,20</sup>, Aminata Touré<sup>3,20,\*</sup>, Valérie Mitchell<sup>13,14,20</sup>, Serge  
9 Amselem<sup>1,12,20,\*\*</sup> and Marie Legendre<sup>1,12,20</sup>

10

11 <sup>1</sup> Sorbonne Université, Institut National de la Santé et de la Recherche Médicale (INSERM U933),  
12 Hôpital Armand-Trousseau, Paris 75012, France.

13 <sup>2</sup> Institute for Integrative Biology of the Cell (I2BC), CEA, CNRS, Univ. Paris-Sud, Université Paris-Saclay,  
14 Gif-sur-Yvette cedex 91198, France.

15 <sup>3</sup> Institut Cochin. Institut National de la Santé et de la Recherche Médicale (INSERM U1016), Centre  
16 National de la Recherche Scientifique (CNRS UMR8104), Université Paris Descartes. Paris 75014,  
17 France.

18 <sup>4</sup> Assistance Publique-Hôpitaux de Paris (AP-HP), Unité Fonctionnelle d'Exploration Fonctionnelle  
19 Respiratoire – Somnologie, Service de Physiologie et Explorations fonctionnelles, Centre National de  
20 Référence des Maladies Respiratoires Rares, Hôpital Armand-Trousseau, Paris 75012, France.

21 <sup>5</sup> Sorbonne Universités, Centre de Recherche Saint-Antoine (CRSA), Paris 75012, France.

22 <sup>6</sup> Assistance Publique-Hôpitaux de Paris (AP-HP), Hôpital Henri Mondor et Centre Hospitalier  
23 Intercommunal de Créteil, service d'Oto-Rhino-Laryngologie et de Chirurgie cervico-faciale, Créteil  
24 94010, France.

25 <sup>7</sup> Université Paris-Est, Faculté de Médecine, Institut National de la Santé et de la Recherche Médicale  
26 (INSERM U955), CNRS ERL7240, Hôpital Henri Mondor, Créteil 94010, France.

27 <sup>8</sup> CHU Lille, Service d’Oto-Rhino-Laryngologie et de Chirurgie cervico-faciale, Hôpital Huriez, Lille  
28 59000, France.

29 <sup>9</sup> Assistance Publique-Hôpitaux de Paris (AP-HP), Service d’Oto-Rhino-Laryngologie et de Chirurgie  
30 cervico-faciale, Hôpital Bicêtre, Le Kremlin-Bicêtre 94275, France.

31 <sup>10</sup> CHU Lille, Services de Pneumologie et Oncologie Thoracique et d’endoscopie respiratoire, Hôpital  
32 Calmette, Lille 59000, France.

33 <sup>11</sup> CHU-Hôpitaux de Rouen, Service de Génétique Médicale, Hôpital Charles Nicolle, Rouen 76000,  
34 France.

35 <sup>12</sup> Assistance Publique-Hôpitaux de Paris (AP-HP), Département de Génétique Médicale, Hôpital  
36 Armand-Trousseau, Paris 75012, France.

37 <sup>13</sup> CHU Lille, Institut de Biologie de la Reproduction-Spermiologie-Cecos, Hôpital Jeanne de Flandre,  
38 Lille 59000, France.

39 <sup>14</sup> EA4308: Gametogenesis and Gamete Quality, Université de Lille, Lille 59000, France.

40 <sup>15</sup> Centre Hospitalier Intercommunal de Créteil, Laboratoire de microscopie électronique, Service  
41 d’Anatomopathologie, Créteil 94010, France.

42 <sup>16</sup> Assistance Publique-Hôpitaux de Paris (AP-HP), Hôpital Cochin, Service de *Pneumologie* et Oncologie  
43 Thoracique, Paris 75014, France.

44 <sup>17</sup> Assistance Publique-Hôpitaux de Paris (AP-HP), Hôpital Henri Mondor et Centre Hospitalier  
45 Intercommunal de Créteil, service de Pneumologie, Créteil 94010, France.

46 <sup>18</sup> Normandie Univ, UNIROUEN, EA 4308 “Gametogenesis and Gamete Quality”, Rouen University  
47 Hospital, Department of Reproductive Biology–CECOS, F 76000 Rouen, France.

48 <sup>19</sup> These authors contributed equally to this work.

49 <sup>20</sup> These authors jointly supervised this work.

50 \* Correspondence: aminata.toure@inserm.fr

51 \*\* Correspondence: serge.amselem@inserm.fr

52 **Abstract**

53 Cilia and flagella are evolutionarily conserved organelles whose motility relies on the outer and inner  
54 dynein arm complexes (ODAs/IDAs). Defects in ODAs/IDAs result in primary ciliary dyskinesia (PCD), a  
55 disease characterized by recurrent airway infections and male infertility. To date PCD mutations in  
56 assembly factors cause a combined ODA/IDA defect, affecting both cilia and flagella. We identified four  
57 loss-of-function mutations in *TTC12*, which encodes a cytoplasmic protein, in four independent  
58 families in which affected individuals displayed a peculiar PCD phenotype characterized by the absence  
59 of ODAs and IDAs in sperm flagella, contrasting with the sole absence of IDAs in respiratory cilia.  
60 Analyses of both primary cells from individuals carrying *TTC12* mutations and human differentiated  
61 airway cells invalidated for *TTC12* by a CRISPR-Cas9 approach revealed an IDA defect restricted to a  
62 subset of single-headed IDAs different in flagella and cilia, while *TTC12* depletion in the ciliate  
63 *Paramecium tetraurelia* recapitulated the sperm phenotype. Overall, our study, which identifies *TTC12*  
64 as a gene involved in PCD, unveils distinct dynein assembly mechanisms in human motile cilia versus  
65 flagella.

## 66 **Introduction**

67 Primary ciliary dyskinesia (PCD [MIM: 244400]) is a group of clinically and genetically heterogeneous  
68 disorders caused by dysfunction of motile cilia leading to impaired mucociliary clearance and early  
69 recurrent airway infections. About one person in 10,000 individuals is concerned<sup>1</sup>, and given the key  
70 role of motile cilia in the establishment of left-right asymmetry during embryogenesis<sup>2</sup>, nearly 50% of  
71 those individuals display a *situs inversus* thereby defining the Kartagener syndrome. In addition, as the  
72 microtubule-based structure of motile cilia, the axoneme, is close to that of sperm flagella, most male  
73 individuals are also infertile. The axoneme consists of nine peripheral outer microtubule doublets  
74 circularly arranged around two central microtubules surrounded by a central sheath (“9+2” pattern).  
75 Attached all along the microtubule length, the outer dynein arms (ODAs) and inner dynein arms (IDAs)  
76 are multiprotein complexes, which carry an ATPase activity and provide the sliding force for motility.  
77 In humans, ODAs are composed of two axonemal dynein heavy chains (HCs), namely the  $\beta$  and  $\gamma$   
78 chains, which are attached to a large intermediate chain/light chain complex (IC/LC). Two types of  
79 ODAs have been described in cilia: the type 1 ODAs are located at the proximal part of the cilium and  
80 contain DNAH5 ( $\gamma$ -chain) associated with DNAH11 ( $\beta$ -chain), while the type 2 ODAs are located at the  
81 distal part of the cilium and contain DNAH5 ( $\gamma$ -chain) associated with DNAH9 ( $\beta$ -chain). Noteworthy,  
82 recent studies performed in humans revealed that the ODA composition of spermatozoa differs from  
83 that found in cilia<sup>3</sup>: in spermatozoa, the  $\gamma$ - and  $\beta$ -chain consist in DNAH8 and DNAH17, respectively,  
84 both being specifically expressed in sperm cells. As for IDAs, their exact structure and composition is  
85 virtually unknown in humans. Most of the knowledge was provided by studies in the flagellated alga  
86 *Chlamydomonas reinhardtii* where seven IDA subspecies have been identified. Six distinct single-  
87 headed IDA subspecies (called IDA a, b, c, d, e, and g), each including only one HC, have been  
88 characterized, and one dimeric IDA complex (called IDA f or IDA-I1), which contains two HCs, has been  
89 identified<sup>4,5,6,7</sup>. There is growing interest in identifying the key players involved in the process of ODA  
90 and IDA assembly and transport. In this regard, one of the most frequent ciliary ultrastructural defects  
91 found in PCD corresponds to the absence of both dynein arms (DAs)<sup>8</sup> due to mutations in genes

92 encoding proteins involved in ODA and IDA assembly, docking and transport (i.e. *DNAAF2/KTU*<sup>9</sup> [MIM:  
93 612517], *DNAAF1/LRRC50*<sup>10</sup> [MIM: 613190], *DNAAF3*<sup>11</sup> [MIM: 614566], *CCDC103*<sup>12</sup> [MIM: 614677],  
94 *DNAAF5/HEATR2*<sup>13</sup> [MIM: 614864], *LRRC6*<sup>14</sup> [MIM: 614930], *DNAAF4/DYX1C1*<sup>15</sup> [MIM: 608709],  
95 *ZMYND10*<sup>16</sup> [MIM: 607070], *SPAG1*<sup>17</sup> [MIM: 603395], *CFAP298/C21orf59*<sup>18</sup> [MIM: 615494], *PIH1D3*<sup>19</sup>  
96 [MIM: 300933] and *CFAP300/C11orf70*<sup>20</sup> [MIM: 618058]).

97 Although several of these genes have been renamed with the acronym DNAAF, which stands for  
98 Dynein Axonemal Assembly Factor, their precise role in the assembly and/or transport machinery is  
99 not known. As shown recently, multiciliated cells contain cytoplasmic liquid-like organelles that  
100 concentrate DNAAFs with dynein chains and chaperones<sup>21</sup>. To date very few investigations have been  
101 performed on spermatozoa from PCD-affected individuals; in all cases, the sperm ultrastructure  
102 defects observed by transmission electron microscopy (TEM) were always found to be identical to  
103 those reported in the cilia. In this regard, the recent observation of differences in protein composition  
104 of ODAs between human cilia and sperm flagella<sup>3</sup> raises the question as to whether the assembly and  
105 transport mechanisms of ODA and IDA components are conserved between human cilia and flagella.

106 In the present study, we identified independent families in which the individuals displayed a peculiar  
107 PCD phenotype characterized by the absence of IDAs in respiratory cilia, contrasting with the absence  
108 of both ODAs and IDAs in sperm. Such unusual observation prompted us to search for the molecular  
109 basis of the PCD phenotype in those individuals and to decipher the consequences of the identified  
110 molecular defects on cilia and flagella assembly, by developing an *in vivo* model in the ciliate  
111 *Paramecium tetraurelia* and a CRISPR-Cas9-mediated genome editing approach in human primary  
112 airway epithelial cells (AECs).

113 **Material and Methods**

114 **Affected individuals**

115 Written informed consent was obtained from all affected individuals and/or their parents following  
116 protocols approved by the Comité de Protection des Personnes (CPP) Ile de France III and the  
117 Institutional Review Board of the French Institute of medical research health (CPP02748 and CEEI-IRB:  
118 opinion number 15-259, respectively).

119

120 **Genetic analyses**

121 Identification of *TTC12* (RefSeq NM\_017868.4) sequence variations was performed from genomic  
122 blood DNA, either by WES or by parallel sequencing with a custom targeted-capture panel. More  
123 precisely, in individual DCP791, WES was performed with the Agilent SureSelect V5 target enrichment  
124 system on a HiSeq sequencing machine (Illumina). In individuals DCP153 and DCP1606, WES was  
125 performed with the SeqCap EZ MedExome target enrichment kit on a NextSeq sequencing machine  
126 (Illumina). The DNA of individual 18GM00157 was analyzed on a MiSeq sequencer (Illumina) with a  
127 custom targeted-capture panel (SeqCap EZ Choice, Roche Diagnostics) that encompasses the 45 genes  
128 involved in PCD and the 250 candidate genes for PCD. The libraries were prepared following  
129 manufacturer's instructions. Data were analyzed through an in-house double pipeline based on  
130 Bowtie2 and BWA tools. Reads were visualized with the IGV viewer (Broad Institute). Copy number  
131 variation analysis was performed with a depth-ratio comparison between subjects sequenced in the  
132 same run, and depth ratios obtained for each of the 4 individuals were represented on a graph built  
133 with the GraphPad Prism 5 software.

134 Sanger sequencing was performed on genomic blood DNA with the BigDye Terminator v3.1 system  
135 (Thermo Fisher) following PCR-amplification with the Go-Taq Green Master Mix (Promega) at an  
136 annealing temperature of 60°C and purification with ExoSAP-IT(USB), following manufacturer's  
137 instructions. Fragments were analyzed on a 3730XL device (Thermo Fisher) after Sephadex G-50

138 Superfine purification (GE Healthcare). Amplification and sequencing primers are listed in **Table S1**.  
139 Sequences were analyzed with the SeqScape software (Thermo Fisher).

140

#### 141 **TEM analysis of ciliary and flagella ultrastructure**

142 AECs obtained from nasal or bronchial biopsies were fixed in 2.5% glutaraldehyde to be processed for  
143 TEM as previously described<sup>22</sup>. Ciliary ultrastructural results were quantified as a percentage of  
144 abnormal cilia among the total number of analyzed cilia. Semen was fixed in 2.0% v/v glutaraldehyde  
145 in phosphate buffer, washed for 15 min in fresh buffer containing 4% w/v sucrose and embedded in  
146 2% agar. Post-fixation lasted 1h in 1% w/v osmic acid in phosphate buffer. After dehydration in a  
147 graded series of ethanol, small pieces of agar containing sperm cells were embedded in Epon resin  
148 (Polysciences Inc., Warrington, PA, USA). Sections were cut on a Reichert OmU2 ultramicrotome  
149 (Reichert-Jung AG, Wien, Austria) using a diamond knife. Sections (70 nm) were collected on nickel  
150 grids and stained with uranyl acetate (2% in 70% ethanol, 20 min) and Reynolds lead citrate (10 min),  
151 and examined using a Zeiss transmission electron microscope 902 (Leo, Rueil-Malmaison, France).  
152 Images were acquired using a Gatan Orius SC1000 CCD camera (Gatan France, Grandchamp, France).

153

#### 154 **Immunoblotting**

155 AECs obtained by airway brushing from individuals 18GM00157, DCP1606 and control individuals, as  
156 well as spermatozoa from a control donor, were suspended in ice-cold lysis buffer (50mM Tris, 150  
157 mM NaCl, 1% Triton X-100, and Complete Protease Inhibitor Cocktail (Roche Diagnostics)). Lysates  
158 were sonicated and cleared by 10 minutes of centrifugation at 1000g, 4°C.

159 Cell lysates were loaded on 10% SDS-PAGE, transferred 2h on a PVDF membrane and analyzed by  
160 western blotting with TTC12 antibody (Santa Cruz sc-390229, 1/200), DNAJB13 antibody (HPA052465,  
161 1/300) or DNAI1 antibody (HPA021649, 1/400), all incubated overnight at 4°C in PBS - 0.1% Tween 20 -  
162 5% milk. The secondary antibody (rabbit-HRP, SIGMA, A0545) was incubated for 1h at room  
163 temperature at a final dilution of 1:5000 in PBS - 0.1% Tween 20 - 5% milk. Proteins were detected



164 using Amersham ECL Select Western Blotting Detection Reagent (GE healthcare) according to the  
165 manufacturer's recommendations.

166

### 167 **Immunofluorescence analyses on AECs**

168 All antibodies are listed in **Table S2**. AECs obtained by nasal brushing from individuals 18GM00157,  
169 DCP1606 and control individuals (i.e. individuals in whom the diagnosis of PCD was excluded on the  
170 basis of the absence of sinopulmonary symptoms and of normal values of nasal nitric oxide) were  
171 suspended in Ferticult IVF medium. Samples were cytocentrifugated onto glass slides, air-dried and  
172 directly used for immunostaining. Cells were first fixed with 4% paraformaldehyde for 15 min at room  
173 temperature, washed three times with PBS supplemented with 0.49mM MgCl<sub>2</sub> and 0.9mM CaCl<sub>2</sub>,  
174 incubated for 10 min with PBS++ NH<sub>4</sub>Cl 50mM, and permeabilized with 0.1% Triton X-100 for 10 min.  
175 Then, cells were incubated 2h at room temperature with primary antibodies before being revealed by  
176 secondary antibodies at room temperature during 1h. All antibodies were incubated in PBS++ 1% BSA.  
177 Cells were finally washed three times with PBS++, mounted in ProLong<sup>®</sup> Gold Antifade Reagent with  
178 DAPI (Cell Signaling #8961) to stain nuclei, and images were taken using an ECLIPSE 80i microscope  
179 (Nikon) with a Retiga-2000R camera (QImaging).

180

### 181 **Immunofluorescence analyses of human spermatozoa**

182 Semen samples were obtained by masturbation after a period of two to seven days of sexual  
183 abstinence, evaluated according to World Health Organization (WHO) guidelines<sup>23</sup> and then frozen  
184 until further analyses. 10µl of frozen semen samples was spread onto a Superfrost Plus slide (Menzel  
185 Glasbearbeitungswerk, GmbH & Co. KG, Braunschweig, Germany) and fixed by incubation with PBS/4%  
186 paraformaldehyde for 10 minutes. The slides were incubated 20 minutes at 95°C in citrate buffer (H-  
187 3300, VectorLabs, Burlingame, CA, USA), treated with 0.2% Triton in PBS for permeabilization and then  
188 blocked by incubation in 1% BSA for 1 hour. The slides were then incubated with primary antibodies  
189 overnight at 4°C and then with secondary antibodies for one hour at room temperature. The slides

190 were mounted in Vectashield medium (Vector Laboratories, Burlingame, USA) supplemented with  
191 0.5mg/ml DAPI and were subsequently analyzed with a Zeiss Axiophot epifluorescence microscope.  
192 Digital images were acquired with a cooled charge-coupled device (CCD) camera (Hamamatsu Co.  
193 Japan), under identical instrument settings, with MetaMorph® software (Molecular Devices, Inc. USA).

#### 194 ***Paramecium* experiments**

195 All experiments were carried out with entirely homozygous mutant strains: 7S strain for feeding  
196 experiments, and nd7 which carries a recessive monogenic mutation blocking trichocyst discharge<sup>24</sup>  
197 for *Paramecium* transformation.

#### 198 - *Paramecium* strain and cultivation

199 Cells were grown at 27 °C in a wheat grass powder (Bio Herbe de Blé L'arbre de vie, Luçay Le Male,  
200 France) infusion medium bacterized with *Klebsiella pneumoniae* and supplemented with 0.8 µg/ml β-  
201 sitosterol according to standard procedures<sup>25</sup>.

#### 202 - *Paramecium* gene knockdown experiments

203 RNAi gene silencing was achieved using the feeding procedure as previously described<sup>26</sup>. Plasmids used  
204 in RNAi silencing experiments were obtained by cloning PCR products, amplified from the coding  
205 region of each gene (**Table S3**), in L4440 vector<sup>27</sup> using Gibson technology (Gibson DJ 2009). These  
206 plasmids were then transformed in HT115 DE3 *Escherichia coli* strain to produce T7Pol-driven dsRNA  
207 as previously described<sup>26</sup>.

#### 208 - Microinjection of a transgene expressing a GFP-tagged TTC12a protein

209 To become resistant to RNAi silencing, the nucleotide sequence from 471 to 745 (corresponding to  
210 dsRNA sequence) of the *TTC12a* coding region was replaced *in vitro* by a modified synthetic DNA  
211 sequence coding for the same amino-acid sequence (**Figure S1**). GFP coding sequence was fused at the  
212 3' end of WT or *TTC12a* resistant-RNAi version and cloned (using Gibson technology (Gibson DJ 2009))  
213 in XhoI site of pPXV-GFP vector under the control of the constitutive regulators of the *Paramecium*  
214 calmodulin gene<sup>28</sup>. Twelve nucleotides coding for four glycine amino acids were introduced between  
215 the *TTC12a* coding region and the GFP coding sequence. The plasmid was linearised by SfiI digestion

216 and microinjected with ND7-complementing plasmid into the macronucleus of nd7-1 mutant cells  
217 unable to discharge their trichocysts<sup>24</sup>. Transformants were first screened for their ability to discharge  
218 trichocysts and if so, further analyzed. Microinjection was made under an inverted Nikon phase-  
219 contrast microscope, using a Narishige micromanipulation device and an Eppendorf air pressure  
220 microinjector.

#### 221 - *Paramecium* TEM analysis

222 For ultrastructural observations, paramecia were permeabilized in PHEM Buffer (PIPES 60 mM, HEPES  
223 25 mM, EGTA 10mM, MgCL2 2 mM, adjusted to pH 6.9 with NaOH) with 1% Triton X100 for 1 min,  
224 rinsed in PHEM Buffer and fixed in 1% (v/v) tannic acid and 1% (v/v) glutaraldehyde in PHEM buffer for  
225 30 min. Cells were then rinsed in PHEM and 0.05 M Cacodylate buffers before being postfixed in 1%  
226 OsO4 (v/v) 0.05 M cacodylate buffer, pH 7.4 for 30 min. After rinsing, cells were embedded into 2%  
227 agarose. Agar blocks were then dehydrated in graded series of ethanol and propylene oxide and  
228 embedded in Epon. Ultrathin sections were contrasted with uranyl acetate and lead citrate. The  
229 sections were examined with Jeol transmission electron microscope 1400 (at 120kV). The number of  
230 ODAs and IDAs were counted in about 140 cilia cross-sections obtained from TTC12-knocked down or  
231 control cells.

#### 232 - *Paramecium* swimming speed and cell trajectory

233 To analyze paramecia swimming behavior of TTC12-depleted and control cells, 8-10 paramecia were  
234 transferred into a drop of conditioned BHB medium and tracked for 10 s every 0.3 s to assess the  
235 swimming pattern under dark field microscopy, using MetaVue software. Image analysis and the  
236 measurement of swimming velocity were then performed with the ImageJ software.

#### 237 - *Paramecium* fluorescence-microscopy analysis

238 Immunofluorescence was performed as follows: paramecia were fixed in 2% paraformaldehyde in  
239 PHEM buffer for 15 min. Cells were then permeabilized for 15 min in 1% Triton X-100 in PHEM and  
240 washed 3 times in PBS/BSA 3%. Immunostaining were performed with polyglutamylated tubulin  
241 antibody (kindly provided by Carsten Janke, 1/500) as previously described<sup>29</sup>. Cells were observed with

242 a confocal Leica SP8 microscope and image stacks were processed with ImageJ and photoshop  
243 softwares.

244

245 - *Paramecium* deciliation, protein extraction and western blot

246 Cilia were purified<sup>30</sup> and recovered by centrifugation at 28,000 × g for 30 min and protein directly  
247 extracted in SDS-Laemmli buffer. Total protein content from paramecia or paramecia cell body  
248 (deciliated paramecia) was directly boiled in 10% SDS followed by dilution in 2XSDS Laemmli buffer.  
249 Proteins were then separated on SDS PAGE, blotted on nylon membrane and probed with an anti-GFP  
250 antibody (1:1,000, Interchim, Montluçon, France).

251

#### 252 **Air-liquid interface (ALI) culture and infection**

253 AECs obtained either from surgical material from non PCD-affected individuals suffering from nasal  
254 polyps requiring surgery or from nasal brushing of PCD-affected individuals, were cultured at ALI as  
255 previously described<sup>31</sup>. Briefly, epithelial cells were seeded in 12-well collagen IV-coated transwell  
256 inserts (Costar, corning) and cultured in PneumaCult-Exp Plus medium (#05040, Stem Cell) until  
257 confluence were reached. The medium was then removed from the apical surface and replaced in the  
258 basal chamber by the PneumaCult-ALI medium (#5001, Stem Cell) in order to expose cells to an air-  
259 liquid interface that promotes ciliogenesis during the following 21 days. Lentiviral transduction of AECs  
260 was performed as previously described<sup>32</sup>. In brief, viral particles were added in the medium together  
261 with a Rho-associated protein kinase inhibitor, during the expansion phase, before a cell selection step  
262 by puromycine (2ug/mL). Resistant cells were then cultured at ALI as described above. Cells infected  
263 with an empty vector were used as control.

264

265 **Results**

266 **Next generation sequencing-based approaches identify homozygous loss-of-function *TTC12***  
267 **mutations in four independent PCD-affected individuals with distinct ciliary and flagellar dynein arm**  
268 **defects**

269 To uncover novel genetic causes responsible for PCD, we used a next generation sequencing (NGS)-  
270 based approach in four independent probands with a PCD phenotype that was not explained by  
271 mutations in genes known to be involved in PCD. As summarized in **Table 1**, individuals DCP791,  
272 18GM00157 and DCP1606, originate from North Africa and were born from a consanguineous union,  
273 whereas the fourth individual, DCP153, originates from Europe with no known consanguinity. All four  
274 individuals displayed sinopulmonary symptoms with rhino-sinusitis and had normal *situs* position.  
275 Individuals 18GM00157 and DCP1606 also displayed bronchiectasis, and individual DCP1606 suffered  
276 from neonatal respiratory distress. Nasal nitric oxide (NO) levels were recorded for those four  
277 individuals, showing low levels for two of them. High-speed videomicroscopy (HSVM) performed on  
278 nasal brushing of three individuals, showed variable proportions of immotile cilia (70%, 50% and 10%  
279 in 18GM00157, DCP1606 and DCP153, respectively), a normal beat frequency and moderate beating  
280 defects (for the portion of motile cilia) consisting of a reduced beating angle and a lower distance  
281 swept by the cilium tip (**Table S1**). Representative movies showing immotile and beating cilia are  
282 shown in supplemental data (**Movies S1-S2, S3-S4, S5-S6** for individuals 18GM00157, DCP1606 and  
283 DCP153, respectively, and **movie S7** for a control individual). TEM analysis of respiratory cilia, which  
284 was performed for individuals DCP153, 18GM00157 and DCP1606, showed the absence of IDAs  
285 associated with some axonemal disorganization (2%, 22% and 24%, respectively) but, importantly, the  
286 presence of ODAs in all examined cilia (**Table 1**) (**Figure 1**).

287 Among the three male individuals, individual DCP1606 was a child (11 year-old) and individuals  
288 DCP791 and DCP153 were adults known to be infertile due to total asthenozoospermia (**Table 2**).  
289 Surprisingly, TEM analysis of sperm cells from the two infertile individuals revealed the total lack of

290 both IDAs and ODAs, an ultrastructural phenotype clearly different from that observed in cilia from  
291 respiratory cells where only IDAs were missing.

292 NGS analyses led to the identification of homozygous mutations in *TTC12* [MIM: 610732], a gene not  
293 associated with PCD so far. *TTC12* is located on chromosome 11 and consists of 22 coding exons  
294 (RefSeq NM\_017868.4) predicting a protein of 705 residues (Uniprot Q9H892). Individuals DCP1606  
295 and 18GM00157 were shown to carry the nonsense mutations c.607del, p.Ile203\* and c.1678C>T,  
296 p.Arg560\*, respectively. Individual DCP791 carries a splice mutation (c.1614+3A>T, p.?) and individual  
297 DCP153 is homozygous for the missense mutation c.1700T>G, p.Met567Arg. Two of these mutations,  
298 c.1614+3A>T and c.607del, are not reported in gnomAD, while the c.1678C>T and c.1700T>G  
299 mutations are found at very low frequencies:  $4 \times 10^{-5}$  and  $6 \times 10^{-5}$ , respectively (**Table S4**). The presence  
300 of all these *TTC12* mutations was confirmed by Sanger sequencing, as illustrated in **Figure S2 and S3**.  
301 The expected consequences of the identified variants at the protein level are shown in **Figure 2**.

302

### 303 ***TTC12* is a cytoplasmic protein of ciliated cells**

304 *TTC12* contains three tetratricopeptide repeat (TPR) domains in its N-terminal part and three armadillo  
305 repeat domains (ARM1, ARM2 and ARM3) in its C-terminal part. A TPR domain consists of a motif of ~  
306 34-aminoacids organized in two antiparallel alpha-helices, known to mediate protein-protein  
307 interactions and the assembly of multiprotein complexes<sup>33</sup>. ARM domains, which are approximately  
308 40-aminoacid long, have also been implicated in protein-protein interactions through their superhelix  
309 structure<sup>34</sup>. To date the biological functions of *TTC12* are unknown. To gain insight into its role, we first  
310 checked *TTC12* tissue expression by RT-PCR in AECs and in testis tissue (**Figure S4A**) with a primer set  
311 (located in exons 2 and 22) bracketing the entire coding region (**Table S1**). Sequencing of the resulting  
312 RT-PCR products allowed the identification of the same *TTC12* isoform (NM\_017868.4) in both  
313 samples. As shown by real-time PCR performed with primers located in exons 11 and 12 of *TTC12*  
314 (**Table S1**), a similar expression level of this transcript was found in AEC and testis samples (**Figure**  
315 **S4B**). The corresponding *TTC12* 75 KDa protein was also easily detectable by western blot in both cell

316 types (**Figure S4C**). We next investigated the subcellular localization of TTC12 in ciliated cells. Given the  
317 absence of available anti-TTC12 antibodies suitable for immunofluorescence (IF) studies, we  
318 performed western blot experiments on protein extracts from ciliary or cytoplasmic fractions of  
319 cultured AECs. This analysis showed that TTC12 is virtually exclusively detected in the cytosolic  
320 fraction, in contrast to DNAJB13, a component of radial spokes which, as expected, was mainly  
321 detected in the ciliary fraction (**Figure S4D**). These results are in line with data from quantitative  
322 proteomic analyses, which did not identify TTC12 in purified preparations of axonemes from human  
323 airway cells<sup>35</sup>. Overall, the cytoplasmic localization of TTC12 indicates that this protein is not a  
324 structural component of the axoneme but would rather play a role in the assembly and/or the  
325 transport of axonemal components.

326

### 327 **Functional consequences of the identified *TTC12* mutations**

328 The nonsense mutations carried by individuals 18GM00157 and DCP1606 might generate truncated  
329 proteins lacking the ARM superhelix structure of TTC12 (**Figure 2**). Such premature stop codons may  
330 also trigger the nonsense-mediated mRNA decay pathway and therefore might lead to the absence of  
331 protein. To test these hypotheses, AECs from individuals 18GM00157 and DCP1606, and from a control  
332 individual were cultured at ALI as previously described<sup>31</sup>. Analysis of total protein extracts by  
333 immunoblotting with an antibody raised against the N-terminal part of TTC12, led to the detection of  
334 the TTC12 protein in the control but not in samples from individuals 18GM00157 and DCP1606 (**Figure**  
335 **3A**). These results clearly indicate that the two nonsense mutations identified in individuals  
336 18GM00157 and DCP1606 are associated with TTC12 loss of function.

337 As for individual DCP153, he carries a missense variation replacing methionine 567, located in the  
338 second ARM domain of TTC12, by an arginine residue. Several lines of evidence support the  
339 involvement of the p.Met567Arg variation in the PCD phenotype of this individual. Firstly, as  
340 mentioned above, this variation is reported in gnomAD at a very low frequency ( $6 \times 10^{-5}$ ) and only in the  
341 heterozygous state (**Table S5**). Secondly, it predicts changes in both the polarity and the charge of this

342 aminoacid highly conserved in mammals. In zebrafish and xenopus, this methionine residue is replaced  
343 by a leucine, an aminoacid also apolar (**Figure S5A**). In addition, alignments of the well-conserved  
344 ARM2 and ARM3 domains of TTC12 with the ten ARM domains found in ARMC4 - also involved in  
345 PCD<sup>36</sup> - unveil (i) that the methionine found in ARM2 at position 567 also corresponds to a methionine  
346 in the ARM3 domain (Met610) (**Figure S5B**), and (ii) the high conservation among all those ARM  
347 domains of a hydrophobic residue at position corresponding to Met567 in TTC12 (**Figure S5C**). Thirdly  
348 and most importantly, when performing western blot analyses on protein extracts from AECs and from  
349 spermatozoa of individual DCP153 who carries the missense mutation in the homozygous state, the  
350 amount of TTC12 was found to be dramatically reduced (**Figure 3A, 4B**), thereby attesting the  
351 pathogenicity of the p.Met567Arg mutation.

352 The last individual, DCP791, carries the c.1614+3A>T transversion involving the splice donor site of  
353 *TTC12* intron 18. As predicted by the MaxEntScan webtool, this nucleotide substitution is expected to  
354 have a strong impact on the splicing of *TTC12* transcripts (score decreasing from 9.49 to 2.03). In  
355 addition, a recent study described a deep neural network that precisely models mRNA splicing from a  
356 genomic sequence and accurately predicts the effects on splicing of all possible genomic SNVs<sup>37</sup>.  
357 Based on this dataset, the probability that the *TTC12* c.1614+3A>T mutation alters the intron 17  
358 canonical splice site is 88%. To further confirm the deleterious effect of this mutation on splicing, we  
359 generated minigene constructs containing a genomic DNA region spanning exons 17 to 19 of *TTC12*,  
360 with or without the A>T transversion. Analysis of the corresponding transcripts in HEK293 cells  
361 transfected with those plasmid constructs showed that the mutation induces a complete skipping of  
362 exon 18 (**Figure S6A, S6B**). This in-frame deletion of exon 18 spares the exons encoding the ARM2 and  
363 ARM3 domains but, as shown with NCBI CDD webtool, the prediction of those domains is lost (**Figure**  
364 **S6C**).

365

### 366 ***TTC12* mutations affect a subset of single-headed IDAs in respiratory cilia**

367 To further investigate the function of *TTC12* in respiratory cilia and in sperm flagella, we first analyzed



368 by high-resolution immunofluorescence the localization of different axonemal components in AECs  
369 from three individuals (18GM00157, DCP1606 and DCP153) compared to controls: DNAH5 and DNAI1  
370 as markers of the ODAs; DNAH2 and DNAH10 for the double-headed IDA-I1 complex; RSPH3 and  
371 RSPH4a for radial spokes (RSs); GAS8 for the nexin-dynein regulatory complex (N-DRC), and CCDC40  
372 for the ciliary ruler<sup>38</sup>. As proposed by Kollmar<sup>39</sup>, the single-headed IDA subspecies (a, b, c, d, e and g)  
373 would result from gene duplications followed by generation of highly divergent N-termini, and  
374 formation, in *Chlamydomonas* but not in mammals, of chimeric single-headed heavy dynein chains.  
375 This model, which relies on thorough phylogenetic analyses, readily explains the fact that the single-  
376 headed IDAs a, c and d bind the light chain DNALI1 (both in *Chlamydomonas* and in humans), while the  
377 heavy chains belonging to another subgroup (b, e and g) bind centrin in *Chlamydomonas*, whereas, in  
378 humans, the b and e heavy chains, which are not chimeric, would bind DNALI1. We therefore  
379 performed immunostaining with antibodies directed against DNALI1 (corresponding to IDA-subspecies  
380 a, c and d, and potentially to IDA subspecies b and e), DNAH1 (corresponding to IDA-subspecies d),  
381 DNAH6 (corresponding to IDA-subspecies g), and DNAH12 and DNAH3, both corresponding to other  
382 IDA subspecies (a, b, c or e). We found that, in the respiratory cilia of the three individuals with *TTC12*  
383 mutations, the subcellular localization patterns of the markers for ODAs, radial spokes (RSs), the nexin-  
384 dynein regulatory complex (N-DRC) and the ciliary ruler were similar to those found in controls (**Figure**  
385 **S7**). Interestingly concerning IDAs, while DNAH2 and DNAH10, corresponding to the double-headed  
386 IDA-I1, were found to be normal in those same three individuals (**Figure S7**), all the markers of the  
387 single-headed IDA subspecies (i.e. DNALI1, DNAH1, DNAH6, and DNAH12) displayed an abnormal  
388 pattern (**Figure 3B**). DNALI1, DNAH1 and DNAH6 were present at low levels in the very proximal part of  
389 the cilia from the three individuals and absent from the rest of the axoneme, while DNAH12 was not  
390 detectable all along the cilia and was found to accumulate at the subapical part of the cytoplasm of  
391 ciliated cells. Overall, in cilia, *TTC12* mutations does not affect ODAs nor IDA-I1, but compromise a  
392 subset of single-headed IDAs which comprises DNALI1, DNAH1, DNAH6, DNAH12. Of note, DNAH3 was  
393 not detected in cilia from control individuals (data not shown).

394

395 ***TTC12* mutations affect ODAs and a distinct subset of single-headed IDAs in sperm flagella**

396 In line with the TEM data, IF analyses in spermatozoa from the infertile PCD-affected individual  
397 DCP153 showed that DNAI1 as well as DNAH8 and DNAH17, the two dynein HCs specific of ODAs in  
398 sperm flagella<sup>3</sup>, were undetectable (**Figure 4A**), thus clearly confirming that *TTC12* mutations induce a  
399 loss of ODAs in sperm cells but not in airway cilia. As very little information on the IDA subtypes and  
400 their HC composition is available in human sperm cells, we analyzed the pattern of all described IDA  
401 HCs in humans (except DNAH7 and DNAH14 for which no antibodies are so far suitable for  
402 immunofluorescence). Interestingly, as observed in cilia, markers of the double-headed IDA-I1 complex  
403 (i.e. DNAH2 and DNAH10) were found unchanged in individual DCP153. Regarding markers of single-  
404 headed IDAs, while the dynein HC DNAH3 (a, b, c or e) was not detected in control respiratory cilia, it  
405 was found present along the axoneme of control spermatozoa. Remarkably, this dynein HC was totally  
406 absent in sperm from individual DCP153. Additionally, DNAH12 (also corresponding to the single-  
407 headed IDA subspecies a, b, c or e) was detected along the full length of the flagellar axoneme in the  
408 control but displayed an expression pattern restricted to the proximal part of the flagella in the  
409 individual (**Figure 4A**). By contrast, the dynein HCs of the single-headed IDA subspecies d and g (i.e.  
410 DNAH1, DNAH6) displayed a normal expression pattern (**Figure S8**). As for the light chain associated  
411 with the IDA subspecies a, c and d (i.e. DNALI1), it was found normally localized along the flagellar  
412 axoneme of spermatozoa from the individual; however, the IF signal intensity appeared to be reduced  
413 (**Figure 4A**), a result confirmed by a western blot performed with an anti-DNALI1 antibody on protein  
414 extracts from the individual's spermatozoa (**Figure 4C**). Taken together, these data demonstrate that in  
415 sperm cells from individuals with *TTC12* mutations, the assembly and/or the transport of ODAs and a  
416 subset of IDAs which comprises DNALI1, DNAH3 and DNAH12, are compromised, while IDA-I1 remains  
417 intact.

418

419 **TTC12-depleted paramecia reproduce the spermatozoa phenotype observed in PCD-affected**  
420 **individuals**

421 To further investigate the function of TTC12 in cilia motility, we undertook studies in the free-living  
422 ciliate *Paramecium tetraurelia* which constitutes a powerful model organism to characterize potential  
423 functions of PCD candidate genes<sup>40,41</sup> as gene functional analysis by RNA interference silencing is rapid,  
424 efficient and easy to perform. Gene homology analyses performed on *P. tetraurelia* genome<sup>28</sup>  
425 identified four genes putatively encoding TTC12 proteins: GSPATT00036969001, GSPATT00034215001,  
426 GSPATT00035675001 and GSPATT00037155001 hereafter named *TTC12a*, *TTC12b*, *TTC12-like a* and  
427 *TTC12-like b*, respectively. Interpro software analysis detected both TPR and ARM repeats, only in  
428 *TTC12a* and *TTC12b*. Therefore, we focused our analysis on these two proteins, which are the closest  
429 orthologs of human TTC12 protein (**Figure S9**). RNAseq analysis showed that *TTC12a* is highly  
430 expressed by contrast to *TTC12b*, and is the only paralog overexpressed during ciliogenesis (**Table**  
431 **S6**<sup>42,43</sup>). By generating a GFP-tagged *TTC12a* protein in paramecia, we showed that, as observed in  
432 human cells, *TTC12a* is a cytoplasmic protein (**Figure S10**). We used the dsRNA feeding method to  
433 silence *TTC12a*, *TTC12b* and the combination *TTC12a+TTC12b*. The knockdown (KD) of *TTC12a* alone or  
434 in association with *TTC12b* led to a dramatic defect in the swimming velocity (**Figure 5A, 5B**) followed  
435 by cell death. By contrast, cells knocked down for *TTC12b* showed no obvious abnormal swimming  
436 phenotype, indicating that only *TTC12a* is essential for cilia motility (**Figure 5A, 5B**). The swimming  
437 velocity and cell death observed in *TTC12a*-depleted cells were rescued by the expression of a  
438 resistant-RNAi version of the gene (**Figure 5C, 5D, 5E**) confirming that the observed phenotypes are  
439 specific to *TTC12* knockdown. Cilia staining immunofluorescence together with TEM indicated that in  
440 *Paramecium TTC12a+b* KD, cilia were globally intact (**Figure 6A**) but contained a reduced number of  
441 ODAs and/or IDAs per cilium (**Figure 6B**). Similar results were obtained after depletion of the *TTC12a*  
442 protein alone (data not shown). Taken together, these data indicate that, similarly to what we found in  
443 human spermatozoa, the assembly and/or transport of both ODAs and IDAs was affected by the

444 absence of TTC12a in the *Paramecium* model, which suggests that the function of this protein is at  
445 least partly conserved throughout evolution.

446

447 **CRISPR-cas9-mediated *TTC12* invalidation in AECs leads to single-headed IDA subspecies defects**  
448 **mimicking the phenotype of AECs from individuals with *TTC12* mutations**

449 In order to further assess the consequences of *TTC12* loss-of-function mutations in airway ciliated  
450 cells, we invalidated *TTC12* in the model of primary AECs cultured at ALI<sup>31</sup> through a CRISPR-cas9  
451 approach. Control AECs were transduced with lentiviruses expressing plentiCRISPRv2 carrying Cas9 and  
452 RNA guides (gRNA) targeting *TTC12*. Two gRNA targeting exon 3 were tested and the most effective  
453 one, gRNA 1 (i.e. with the higher level of insertions or deletions, as assessed by TIDE webtool), was  
454 used for further experiments. Genomic DNA (gDNA) was then extracted from ALI cultures transduced  
455 with gRNA 1. We found that 82% of gDNA carried INDELS, including 28% of single-nucleotide insertions  
456 (**Figure S11A, S11B**). *TTC12* invalidation in AECs was confirmed by western blot (**Figure S11C**), thereby  
457 allowing us to investigate the functional effects of such invalidation on the main axonemal  
458 components. Immunofluorescence staining of *TTC12*-invalidated cultured epithelial cells revealed a  
459 phenotype similar to that found in primary cells from individuals with *TTC12* mutations: only axonemal  
460 components specific of single-headed IDAs (i.e. DNAH1, DNAH6, DNAH12 and DNALI1) were found to  
461 be affected (**Figure 7A, 7B**). More specifically, the analysis of ciliated cells cultured in ALI by high-  
462 resolution IF confirmed the invalidation of *TTC12* in clusters with a combination of ciliated cells lacking  
463 DNAH6, DNAH12 and DNALI1 along the cilia length, and ciliated cells with normal staining (**Figure 7A**).  
464 Moreover, analysis of isolated ciliated cells confirmed the data obtained in AECs from individuals with  
465 *TTC12* mutations, with the abnormal localization of DNAH1, DNAH6 and DNALI1, found at very low  
466 levels at the base of the cilia, while DNAH12 was completely absent all along the cilia (**Figure 7B**). All  
467 the other tested axonemal components displayed a normal staining (i.e. DNAH5, DNAH9, DNAH11 and  
468 DNAI1 for ODAs; DNAH2 and DNAH10 for IDA-I1; RSPH1, RSPH3, RSPH4a, RSPH9 and RSPH11 for RSs;  
469 GAS8 for the N-DRC, and CCDC39 and CCDC40 for the ciliary ruler) indicating that all other axonemal

470 complexes were normally assembled (**Figure S12**). To further study the impact of *TTC2* invalidation on  
471 ciliary axonemal components, cross-sections of cilia from *TTC12*-invalidated epithelial cells were  
472 analyzed by TEM. As shown in **Figure 7C**, those cilia displayed an abnormal ultrastructure with 84% of  
473 cilia lacking IDAs, whereas a non-infected culture harbored only 3% of abnormal cilia. This  
474 ultrastructural phenotype correlates again with the one found in individuals with *TTC12* mutations.

475 **Discussion**

476 We report mutations in *TTC12*, a gene encoding a protein involved in cytoplasmic assembly and/or  
477 transport of axonemal dynein arms, in PCD-affected individuals. A thorough analysis of the phenotype  
478 of sperm flagella and respiratory cilia from *TTC12*-deficient individuals revealed that the loss of  
479 function of *TTC12* affects both ODAs and a subset of single-headed IDAs in sperm flagella, but only a  
480 different subset of single-headed IDAs in respiratory cilia. These data, which are further supported by  
481 two cellular models of the pathology (i.e. the ciliate *Paramecium tetraurelia* depleted in *TTC12* and  
482 human AECs differentiated *in vitro* after a CRISPR-cas9-mediated invalidation of *TTC12*), reveal the  
483 existence of distinct dynein assembly mechanisms in human sperm flagella and respiratory cilia.

484 The biological function of *TTC12* is still elusive. One study has shown an upregulation of *TTC12*  
485 transcripts during mouse ciliogenesis *in vitro* and a centrosomal localization of *TTC12* fused to GFP<sup>44</sup>. In  
486 paramecia, *TTC12a*, the ortholog of human *TTC12*, was also found to be overexpressed during  
487 ciliogenesis (*ParameciumDB*). While some TTC proteins have been involved in the so-called intra  
488 flagellar transport (IFT)<sup>45-47</sup>, as for *TTC12*, the following characteristics support its possible role as a co-  
489 chaperone: (i) *TTC12* contains three TPR domains and three ARM domains, two structural motifs with  
490 alpha helices known to be involved in protein-protein interactions; and TPR-containing proteins are  
491 part of several multiprotein complexes that include co-chaperones<sup>33</sup>; (ii) noteworthy, in humans, only  
492 two other proteins are known to contain both TPR and ARM domains: UNC45A and UNC45B that have  
493 been shown to interact with HSP90 and to act as molecular co-chaperones<sup>34,48-50</sup>. These data, together  
494 with the cytoplasmic localization of *TTC12*, are therefore consistent with a role of *TTC12* as a co-  
495 chaperone involved in dynein assembly.

496 The cytoplasmic assembly of DAs is a complex process involving a wide and still incompletely resolved  
497 chaperone-mediated protein network. Dynein arm components are first synthesized and pre-  
498 assembled into multi-subunit structures in the cytoplasm, before being transported by IFT into the  
499 axoneme for microtubule attachment<sup>51,52</sup>. Except HSP90, all the proteins known to be involved in the  
500 axonemal dynein pre-assembly network have been implicated in PCD (i.e. CFAP300, CFAP298,

501 CCDC103, DAAAF1, DAAAF2, DAAAF3, DAAAF4, DAAAF5, LRRC6, PIH1D3, SPAG1 and ZMYND10).  
502 HSP90 is known to interact with TPR domains of various co-chaperones to promote their function<sup>53</sup>.  
503 Two so-called dynein assembly factors contain TPR domains: DAAAF4 and SPAG1. In recent studies,  
504 DAAAF4 was found to interact with both HSP90 and DAAAF2 through its TPR domains to form an  
505 R2TP-like complex<sup>54,55</sup>. PIH1D3, whose corresponding gene has recently been involved in PCD, might  
506 also interact with HSP90 through a TPR-containing protein which could be DAAAF4<sup>54,55</sup>. Interestingly,  
507 DAAAF4, which seems to play a central role in this network, was found to interact with ZMYND10, a  
508 partner of LRRC6 and CFAP298<sup>16,56</sup>, while the latter one also interacts with DAAAF1<sup>57</sup>. In this assembly  
509 network, it has been reported that DAAAF2 and PIH1D3 interact with DNAI2<sup>9,55</sup>, a dynein intermediate  
510 chain known to assemble early in the human ODA assembly process<sup>58</sup>. As for DAAAF5, it has been  
511 shown to interact with DNAI2, but would not bind HSP90<sup>58</sup>. Regarding CFAP300, DAAAF3, SPAG1 and  
512 CCDC103, their functions remain unclear with so far no reported interactions with HSP90 or other  
513 chaperones. In this context, TTC12, with its three TPR domains that suggest an interaction with HSP90  
514 and/or other chaperones, emerges as a player in this complex pre-assembly network.

515 In most studies, the absence of both DAs in PCD-affected individuals has been identified by TEM  
516 together with high-resolution IF using mainly DNAH5 and DNALI1 antibodies directed against the ODA  
517  $\gamma$ -heavy chain and a/c/d IDA subspecies, respectively. However, these two approaches do not allow  
518 determining which ODA type(s) and which IDA subspecies are affected. For *DAAAF4*, *DAAAF5* and  
519 *CCDC103* mutations, which are responsible for an absence of both DAs, the proximal staining of  
520 DNAH5 and DNAI2 and/or the loss of DNAH9 staining suggest that only type 2 ODAs are affected<sup>9,12,15</sup>.

521 In order to accurately decipher the role played by TTC12 in dynein arm assembly, we aimed to identify  
522 which single-headed IDA subspecies are affected in respiratory cilia of individuals with *TTC12*  
523 mutations. Besides the presence of ODAs, as attested to by TEM and immunofluorescence analyses,  
524 IDA staining revealed that IDA-I1 remained present while, according to the *Chlamydomonas* model,  
525 four of the six single-headed IDA subspecies were affected: a, c, d and g.  
526 No conclusion could be raised on b and e subspecies since the heavy chain DNAH12 is so far not

527 assigned to a specific subspecies (a, or b, or c, or e), and no efficient antibodies are available to detect  
528 the two remaining IDA heavy chains (i.e. DNAH7 and DNAH14) (**Figure 8**). Of note, proteomic analyses  
529 performed on human airway cilia and spermatozoa showed that DNAH7 is present in both proteomes,  
530 unlike DNAH14 that is undetected in both of them<sup>35,59-61</sup>. Like in cilia, spermatozoa from individuals  
531 with *TTC12* mutations conserve the dimeric IDA-I1. Nonetheless, unlike cilia, those spermatozoa  
532 display an absence of ODAs as revealed by TEM analyses and confirmed by the absence of staining of  
533 the ODA HCs specifically expressed in flagella (DNAH8 and DNAH17)<sup>3</sup>. Interestingly, as for single-  
534 headed IDA components, our results show that the IDA heavy chain DNAH3 (present in the IDA  
535 subspecies a, b, c, or e) is detected in flagellar axonemes, whereas, it is not detectable in cilia as  
536 expected from proteomic data<sup>35,59</sup>. Additionally, spermatozoa from an individual with biallelic *TTC12*  
537 mutations displayed a loss of DNAH3 together with a mislocalization of DNAH12 (another monomeric  
538 IDA heavy chain not specifically assigned to subspecies a, b, c or e), thereby unveiling the role of *TTC12*  
539 in the proper expression of DNAH3 and DNAH12 in sperm cells.

540 Surprisingly, although DNAH1 (d) and DNAH6 (g) are present in both normal cilia and flagella, they  
541 were not impacted by *TTC12* mutations in spermatozoa, contrasting with what was observed in cilia.  
542 Moreover, in those spermatozoa, DNALI1 amounts were found reduced but present (**Figure 8**).

543 Taken together, these results show that, in spermatozoa, *TTC12* defects lead to the complete absence  
544 of ODAs and of a set of monomeric IDA subspecies, which is different from the one impacted in  
545 respiratory cilia. While the absence of ODAs in flagella could be explained by differences in ODA  
546 composition between cilia and flagella (DNAH5/DNAH9/DNAH11 and DNAH8/DNAH17, respectively),  
547 the differences affecting single-headed IDAs are not exclusively due to distinct dynein HC composition  
548 (e.g. DNAH1 and DNAH6 are both present in cilia and flagella).

549 In paramecia, *TTC12* knock-down led to the absence of both dynein arms and to a drastic impairment  
550 of the swimming velocity. This suggests similarities in the ODA/IDA assembly process at play in this  
551 protist and in human sperm flagella. In human cilia, except for *TTC12*, the defects of all known co-  
552 chaperones affect both ODAs and IDAs. The situation is very different in *Chlamydomonas* where



553 several of the algal homolog genes are important for assembly of one dynein arm type: *DNAAF1* and  
554 *HEATR2* homologs (i.e. *ODA7* and *HEATR2*, respectively) govern the assembly of ODAs only, whereas  
555 the *DNAAF4* homolog (i.e. *PF23*) contributes only to the assembly of some IDAs<sup>62</sup>.

556 As paramecia mimicked the human flagellar phenotype but not the ciliary one, we looked for an  
557 additional cellular model to further strengthen our conclusions on the role of *TTC12* in cilia. We  
558 developed a human differentiated cell culture model based on CRISPR-cas9 invalidation of *TTC12*.  
559 Primary AECs cultured under ALI conditions constitute a strong epithelial barrier very difficult to  
560 efficiently transfect, especially without inhibiting ciliogenesis. In this study, we show that transduction  
561 of AECs during their expansion phase is not only highly efficient, but, most importantly, it also  
562 preserves ciliogenesis, providing large amounts of ciliated cells from which DNA, RNA and protein  
563 expression can be studied. After puromycin selection, 100% of cultured cells were infected, but four  
564 populations with different genotypes might be present: no indel in *TTC12*, indels within one *TTC12*  
565 allele, distinct indels within each of the two *TTC12* alleles, or the same indel within the two *TTC12*  
566 alleles, equivalent to a wild-type genotype at the *TTC12* locus or a *TTC12* loss-of-function mutation  
567 present in the heterozygous, compound heterozygous or homozygous state, respectively. Since AECs  
568 cannot be dissociated and isolated for selection, contrary to what is done for cell lines, we had to work  
569 with a heterogeneous population of cells invalidated or not for *TTC12*. Nevertheless, our results  
570 revealed that *TTC12* CRISPR AECs perfectly mimic the phenotype observed in cilia from individuals  
571 carrying *TTC12* mutations, while *TTC12*-KD paramecia displayed a ciliary phenotype closer to the  
572 flagellar phenotype observed in human spermatozoa. From a general viewpoint, this demonstrates  
573 that CRISPR-cas9-engineered AECs represent a valuable model to study the impact of PCD mutations  
574 on ciliary axonemes.

575 As for clinical aspects, the diagnosis of PCD is difficult to establish in individuals with mild respiratory  
576 symptoms and no laterality defect. In such situations, low levels of nasal NO, an abnormal ciliary beat  
577 frequency and/or the presence of ciliary ultrastructural defects are essential to confirm or not the  
578 suspicion of PCD. In the current study, all the individuals were exempt of laterality defects and

579 displayed motile cilia with a normal beat frequency. In two of them, nasal NO values were normal.  
580 Furthermore, the ciliary ultrastructural defect (i.e. isolated absence of IDAs with an inconstant and  
581 mild axonemal disorganization) was also difficult to assert by TEM because of the usual low contrast of  
582 IDAs. The diagnosis of PCD was, however, much easier to establish in the two adult male individuals  
583 given their infertility due to a sperm immotility related to the flagellar absence of both DAs, an  
584 ultrastructural defect easily identified by TEM. It is therefore tempting to speculate that PCD could be  
585 underdiagnosed in female individuals with *TTC12* mutations, in young male individuals or in adult  
586 males in whom no TEM analyses of their spermatozoa is performed, thereby underscoring the major  
587 interest of molecular analyses in such individuals.

588 In conclusion, *TTC12* emerges as a cytoplasmic player in dynein arm assembly and/or transport. So far,  
589 all the mutations in genes encoding cytoplasmic pre-assembly factors cause a combined ODA and IDA  
590 defect. However, *TTC12* mutations lead to distinct ultrastructural defects in cilia (i.e. absence of  
591 single-headed IDAs) and in sperm flagella (i.e. absence of both dynein arms), which unveils its role as a  
592 possible co-chaperone in charge of monomeric IDAs in both organelles but not of ODAs in cilia. More  
593 precisely, *TTC12* is in charge of different dynein heavy chains in monomeric IDAs from cilia and from  
594 flagella. Furthermore, our findings should be of particular help to establish the diagnosis of PCD in  
595 individuals with isolated IDA defects in respiratory cilia. The development of a cellular model based on  
596 human AECs differentiated *in vitro* into ciliated cells after a CRISPR-cas9-mediated invalidation of  
597 genes of interest should open new avenues to decipher both the role of the numerous proteins  
598 expressed during ciliogenesis and the pathophysiology of diseases of the airway epithelium.

599

600 **SUPPLEMENTAL DATA**

601 Supplemental data include 12 figures, 6 tables and 7 movies.

602 **ACKNOWLEDGEMENTS**

603 We are grateful to the affected persons and their families, whose cooperation made this study  
604 possible. We acknowledge the contributions of the CELPHEDIA Infrastructure  
605 (<http://www.celphedia.eu/>), especially the center AniRA in Lyon and Gisèle Froment, Didier Nègre and  
606 Caroline Costa from the lentivectors production facility / SFR Biosciences Gerland – Lyon Sud  
607 (UMS3444/US8) and RaDiCo funded by the French National Research Agency under the specific  
608 programme “Investments for the Future”, Cohort grant agreement ANR-10-COHO-0003. We thank  
609 Lucas Fares-Taie and Araksya Izmiryan at IMAGINE Institute for their advice in setting up the CRISPR-  
610 cas9 technology. We thank Anne Loyens from INSERM U1172 at Lille University for TEM technical  
611 assistance and Feng Zhang (Massachusetts Institute of Technology) for the gift of the plentiCRISPRv2  
612 plasmid.

613

614 **DECLARATION OF INTERESTS**

615 The authors declare no competing interests.

616

617 **WEB RESSOURCES**

618 Conserved Domain Database (NCBI CDD webtool), <https://www.ncbi.nlm.nih.gov/cdd/>

619 Clustal Omega program, <http://www.ebi.ac.uk/Tools/msa/clustalo/>

620 CRISPOR TEFOR, <http://crispor.tefor.net/>

621 EMBL EBI Expression Atlas, <http://www.ebi.ac.uk/gxa/home>

622 EMBL EBI Ensembl, <http://www.ensembl.org/index.html>

623 GnomAD, <https://gnomad.broadinstitute.org/>

624 InterPro, <https://www.ebi.ac.uk/interpro/>

- 625 OMIM, <http://www.omim.org/>
- 626 *Paramecium*DB, <https://paramecium.i2bc.paris-saclay.fr>
- 627 SMART, <http://smart.embl-heidelberg.de/>
- 628 TIDE, <https://tide.deskgen.com/>
- 629 Uniprot, <https://www.uniprot.org/>

630 1. Lucas, J.S., Burgess, A., Mitchison, H.M., Moya, E., Williamson, M., Hogg, C., and National PCD  
631 Service, UK (2014). Diagnosis and management of primary ciliary dyskinesia. *Arch. Dis. Child.* *99*, 850–  
632 856.

633 2. Dasgupta, A., and Amack, J.D. (2016). Cilia in vertebrate left–right patterning. *Philosophical*  
634 *Transactions of the Royal Society B: Biological Sciences* *371*, 20150410.

635 3. Whitfield, M., Thomas, L., Bequignon, E., Schmitt, A., Stouvenel, L., Montantin, G., Tissier, S.,  
636 Duquesnoy, P., Copin, B., Chantot, S., et al. (2019). Mutations in DNAH17, Encoding a Sperm-Specific  
637 Axonemal Outer Dynein Arm Heavy Chain, Cause Isolated Male Infertility Due to Asthenozoospermia.  
638 *The American Journal of Human Genetics*.

639 4. Bui, K.H., Yagi, T., Yamamoto, R., Kamiya, R., and Ishikawa, T. (2012). Polarity and asymmetry in the  
640 arrangement of dynein and related structures in the *Chlamydomonas* axoneme. *The Journal of Cell*  
641 *Biology* *198*, 913–925.

642 5. Lin, J., Yin, W., Smith, M.C., Song, K., Leigh, M.W., Zariwala, M.A., Knowles, M.R., Ostrowski, L.E., and  
643 Nicastro, D. (2014). Cryo-electron tomography reveals ciliary defects underlying human RSPH1 primary  
644 ciliary dyskinesia. *Nature Communications* *5*,.

645 6. Viswanadha, R., Sale, W.S., and Porter, M.E. (2017). Ciliary Motility: Regulation of Axonemal Dynein  
646 Motors. *Cold Spring Harbor Perspectives in Biology* *9*, a018325.

647 7. Hom, E.F.Y., Witman, G.B., Harris, E.H., Dutcher, S.K., Kamiya, R., Mitchell, D.R., Pazour, G.J., Porter,  
648 M.E., Sale, W.S., Wirschell, M., et al. (2011). A unified taxonomy for ciliary dyneins. *Cytoskeleton* *68*,  
649 555–565.

650 8. Lucas, J.S., Barbato, A., Collins, S.A., Goutaki, M., Behan, L., Caudri, D., Dell, S., Eber, E., Escudier, E.,  
651 Hirst, R.A., et al. (2017). European Respiratory Society guidelines for the diagnosis of primary ciliary  
652 dyskinesia. *European Respiratory Journal* *49*, 1601090.

653 9. Omran, H., Kobayashi, D., Olbrich, H., Tsukahara, T., Loges, N.T., Hagiwara, H., Zhang, Q., Leblond,  
654 G., O’Toole, E., Hara, C., et al. (2008). Ktu/PF13 is required for cytoplasmic pre-assembly of axonemal  
655 dyneins. *Nature* *456*, 611–616.

656 10. Duquesnoy, P., Escudier, E., Vincensini, L., Freshour, J., Bridoux, A.-M., Coste, A., Deschildre, A., de  
657 Blic, J., Legendre, M., Montantin, G., et al. (2009). Loss-of-Function Mutations in the Human Ortholog  
658 of *Chlamydomonas reinhardtii* ODA7 Disrupt Dynein Arm Assembly and Cause Primary Ciliary  
659 Dyskinesia. *Am J Hum Genet* 85, 890–896.

660 11. Mitchison, H.M., Schmidts, M., Loges, N.T., Freshour, J., Dritsoula, A., Hirst, R.A., O’Callaghan, C.,  
661 Blau, H., Al Dabbagh, M., Olbrich, H., et al. (2012). Mutations in axonemal dynein assembly factor  
662 DNAAF3 cause primary ciliary dyskinesia. *Nature Genetics* 44, 381–389.

663 12. Panizzi, J.R., Becker-Heck, A., Castleman, V.H., Al-Mutairi, D., Liu, Y., Loges, N.T., Pathak, N., Austin-  
664 Tse, C., Sheridan, E., Schmidts, M., et al. (2012). CCDC103 mutations cause primary ciliary dyskinesia by  
665 disrupting assembly of ciliary dynein arms. *Nat Genet* 44, 714–719.

666 13. Horani, A., Druley, T.E., Zariwala, M.A., Patel, A.C., Levinson, B.T., Van Arendonk, L.G., Thornton,  
667 K.C., Giacalone, J.C., Albee, A.J., Wilson, K.S., et al. (2012). Whole-Exome Capture and Sequencing  
668 Identifies HEATR2 Mutation as a Cause of Primary Ciliary Dyskinesia. *The American Journal of Human*  
669 *Genetics* 91, 685–693.

670 14. Kott, E., Duquesnoy, P., Copin, B., Legendre, M., Dastot-Le Moal, F., Montantin, G., Jeanson, L.,  
671 Tamalet, A., Papon, J.-F., Siffroi, J.-P., et al. (2012). Loss-of-Function Mutations in LRRC6, a Gene  
672 Essential for Proper Axonemal Assembly of Inner and Outer Dynein Arms, Cause Primary Ciliary  
673 Dyskinesia. *Am J Hum Genet* 91, 958–964.

674 15. Tarkar, A., Slagle, C.E., Francis, R., Dougherty, G.W., Tamayo, J.V., Shook, B., Cantino, M., Schwartz,  
675 D., Jahnke, C., Olbrich, H., et al. (2013). DYX1C1 is required for axonemal dynein assembly and ciliary  
676 motility. *Nature Genetics* 45, 995–1003.

677 16. Zariwala, M.A., Gee, H.Y., Kurkowiak, M., Al-Mutairi, D.A., Leigh, M.W., Hurd, T.W., Hjeij, R., Dell,  
678 S.D., Chaki, M., Dougherty, G.W., et al. (2013). ZMYND10 Is Mutated in Primary Ciliary Dyskinesia and  
679 Interacts with LRRC6. *Am J Hum Genet* 93, 336–345.

680 17. Knowles, M.R., Ostrowski, L.E., Loges, N.T., Hurd, T., Leigh, M.W., Huang, L., Wolf, W.E., Carson,  
681 J.L., Hazucha, M.J., Yin, W., et al. (2013). Mutations in SPAG1 Cause Primary Ciliary Dyskinesia

682 Associated with Defective Outer and Inner Dynein Arms. *The American Journal of Human Genetics* 93,  
683 711–720.

684 18. Austin-Tse, C., Halbritter, J., Zariwala, M.A., Gilberti, R.M., Gee, H.Y., Hellman, N., Pathak, N., Liu, Y.,  
685 Panizzi, J.R., Patel-King, R.S., et al. (2013). Zebrafish Ciliopathy Screen Plus Human Mutational Analysis  
686 Identifies C21orf59 and CCDC65 Defects as Causing Primary Ciliary Dyskinesia. *The American Journal of*  
687 *Human Genetics* 93, 672–686.

688 19. Paff, T., Loges, N.T., Aprea, I., Wu, K., Bakey, Z., Haarman, E.G., Daniels, J.M.A., Sijm, E.A.,  
689 Bogunovic, N., Dougherty, G.W., et al. (2017). Mutations in PIH1D3 Cause X-Linked Primary Ciliary  
690 Dyskinesia with Outer and Inner Dynein Arm Defects. *The American Journal of Human Genetics* 100,  
691 160–168.

692 20. Höben, I.M., Hjeij, R., Olbrich, H., Dougherty, G.W., Nöthe-Menchen, T., Aprea, I., Frank, D.,  
693 Pennekamp, P., Dworniczak, B., Wallmeier, J., et al. (2018). Mutations in C11orf70 Cause Primary  
694 Ciliary Dyskinesia with Randomization of Left/Right Body Asymmetry Due to Defects of Outer and  
695 Inner Dynein Arms. *The American Journal of Human Genetics* 102, 973–984.

696 21. Huizar, R.L., Lee, C., Boulgakov, A.A., Horani, A., Tu, F., Marcotte, E.M., Brody, S.L., and Wallingford,  
697 J.B. (2018). A liquid-like organelle at the root of motile ciliopathy. *ELife* 7,.

698 22. Verra, F., Fleury-Feith, J., Boucherat, M., Pinchon, M.-C., Bignon, J., and Escudier, E. (1993). Do  
699 Nasal Ciliary Changes Reflect Bronchial Changes?: An Ultrastructural Study. *Am Rev Respir Dis* 147,  
700 908–913.

701 23. Cooper, T.G., Noonan, E., von Eckardstein, S., Auger, J., Baker, H.W.G., Behre, H.M., Haugen, T.B.,  
702 Kruger, T., Wang, C., Mbizvo, M.T., et al. (2010). World Health Organization reference values for  
703 human semen characteristics\*. *Human Reproduction Update* 16, 231–245.

704 24. Skouri, F., and Cohen, J. (1997). Genetic approach to regulated exocytosis using functional  
705 complementation in *Paramecium*: identification of the ND7 gene required for membrane fusion. *Mol.*  
706 *Biol. Cell* 8, 1063–1071.

707 25. Sonneborn, T.M. (1970). Chapter 12 Methods in Paramecium Research\*\*With contributed sections  
708 by: S. Dryl, Nencki Institute of Experimental Biology, Warsaw, Poland; E. D. Hanson, Connecticut  
709 Wesleyan University, Middletown, Connecticut; K. Hiwatashi, Tôhoku University, Sendai, Japan; S.  
710 Koizumi, University of Iwate, Ueda Morioka, Japan; A. Miyake, Kyoto University, Kyoto, Japan; J. R.  
711 Preer, Jr., Indiana University, Bloomington, Indiana; A. Reisner, CSIRO, division of Animal Genetics,  
712 Epping, New South Wales; E. Steers, Department of Health, Education and Welfare, National Institute  
713 of Health, Bethesda, Maryland; S. Taub, Princeton University, Princeton, New Jersey. In *Methods in Cell*  
714 *Biology*, D.M. Prescott, ed. (Academic Press), pp. 241–339.

715 26. Galvani, A., and Sperling, L. (2002). RNA interference by feeding in Paramecium. *Trends Genet.* *18*,  
716 11–12.

717 27. Timmons, L., and Fire, A. (1998). Specific interference by ingested dsRNA. *Nature* *395*, 854.

718 28. Hauser, K., Haynes, W.J., Kung, C., Plattner, H., and Kissmehl, R. (2000). Expression of the green  
719 fluorescent protein in Paramecium tetraurelia. *Eur. J. Cell Biol.* *79*, 144–149.

720 29. Rüdiger, A.H., Rüdiger, M., Wehland, J., and Weber, K. (1999). Monoclonal antibody ID5: epitope  
721 characterization and minimal requirements for the recognition of polyglutamylated alpha- and beta-  
722 tubulin. *Eur. J. Cell Biol.* *78*, 15–20.

723 30. Adoutte, A., Ramanathan, R., Lewis, R.M., Dute, R.R., Ling, K.Y., Kung, C., and Nelson, D.L. (1980).  
724 Biochemical studies of the excitable membrane of Paramecium tetraurelia. III. Proteins of cilia and  
725 ciliary membranes. *J. Cell Biol.* *84*, 717–738.

726 31. Coste, A., Brugel, L., Maitre, B., Boussat, S., Papon, J.F., Wingerstmann, L., Peynegre, R., and  
727 Escudier, E. (2000). Inflammatory cells as well as epithelial cells in nasal polyps express vascular  
728 endothelial growth factor. *European Respiratory Journal* *15*, 367–372.

729 32. Horani, A., Nath, A., Wasserman, M.G., Huang, T., and Brody, S.L. (2013). Rho-Associated Protein  
730 Kinase Inhibition Enhances Airway Epithelial Basal-Cell Proliferation and Lentivirus Transduction. *Am J*  
731 *Respir Cell Mol Biol* *49*, 341–347.



732 33. Blatch, G.L., and Lässle, M. (1999). The tetratricopeptide repeat: a structural motif mediating  
733 protein-protein interactions. *BioEssays* 21, 932–939.

734 34. Tewari, R., Bailes, E., Bunting, K.A., and Coates, J.C. (2010). Armadillo-repeat protein functions:  
735 questions for little creatures. *Trends in Cell Biology* 20, 470–481.

736 35. Blackburn, K., Bustamante-Marin, X., Yin, W., Goshe, M.B., and Ostrowski, L.E. (2017). Quantitative  
737 Proteomic Analysis of Human Airway Cilia Identifies Previously Uncharacterized Proteins of High  
738 Abundance. *Journal of Proteome Research* 16, 1579–1592.

739 36. Hjeij, R., Lindstrand, A., Francis, R., Zariwala, M.A., Liu, X., Li, Y., Damerla, R., Dougherty, G.W.,  
740 Abouhamed, M., Olbrich, H., et al. (2013). ARMC4 Mutations Cause Primary Ciliary Dyskinesia with  
741 Randomization of Left/Right Body Asymmetry. *The American Journal of Human Genetics* 93, 357–367.

742 37. Jaganathan, K., Kyriazopoulou Panagiotopoulou, S., McRae, J.F., Darbandi, S.F., Knowles, D., Li, Y.I.,  
743 Kosmicki, J.A., Arbelaez, J., Cui, W., Schwartz, G.B., et al. (2019). Predicting Splicing from Primary  
744 Sequence with Deep Learning. *Cell* 176, 535-548.e24.

745 38. Osinka, A., Poprzeczko, M., Zielinska, M.M., Fabczak, H., Joachimiak, E., and Wloga, D. (2019).  
746 Ciliary Proteins: Filling the Gaps. Recent Advances in Deciphering the Protein Composition of Motile  
747 Ciliary Complexes. *Cells* 8, 730.

748 39. Kollmar, M. (2016). Fine-Tuning Motile Cilia and Flagella: Evolution of the Dynein Motor Proteins  
749 from Plants to Humans at High Resolution. *Molecular Biology and Evolution* 33, 3249–3267.

750 40. Fassad, M.R., Shoemark, A., Legendre, M., Hirst, R.A., Koll, F., le Borgne, P., Louis, B., Daudvohra, F.,  
751 Patel, M.P., Thomas, L., et al. (2018). Mutations in Outer Dynein Arm Heavy Chain DNAH9 Cause Motile  
752 Cilia Defects and Situs Inversus. *Am. J. Hum. Genet.* 103, 984–994.

753 41. Fassad, M.R., Shoemark, A., le Borgne, P., Koll, F., Patel, M., Dixon, M., Hayward, J., Richardson, C.,  
754 Frost, E., Jenkins, L., et al. (2018). C11orf70 Mutations Disrupting the Intraflagellar Transport-  
755 Dependent Assembly of Multiple Axonemal Dyneins Cause Primary Ciliary Dyskinesia. *Am. J. Hum.*  
756 *Genet.* 102, 956–972.

757 42. Arnaiz, O., Malinowska, A., Klotz, C., Sperling, L., Dadlez, M., Koll, F., and Cohen, J. (2009). Cildb: a  
758 knowledgebase for centrosomes and cilia. Database (Oxford) 2009, bap022.

759 43. Remodeling Cildb, a popular database for cilia and links for ciliopathies. - PubMed - NCBI.

760 44. Hoh, R.A., Stowe, T.R., Turk, E., and Stearns, T. (2012). Transcriptional Program of Ciliated Epithelial  
761 Cells Reveals New Cilium and Centrosome Components and Links to Human Disease. PLoS One 7,.

762 45. Xu, Y., Cao, J., Huang, S., Feng, D., Zhang, W., Zhu, X., and Yan, X. (2015). Characterization of  
763 Tetratricopeptide Repeat-Containing Proteins Critical for Cilia Formation and Function. PLOS ONE 10,  
764 e0124378.

765 46. Pazour, G.J., Dickert, B.L., Vucica, Y., Seeley, E.S., Rosenbaum, J.L., Witman, G.B., and Cole, D.G.  
766 (2000). *Chlamydomonas* IFT 88 and Its Mouse Homologue, Polycystic Kidney Disease Gene *Tg* 737, Are  
767 Required for Assembly of Cilia and Flagella. The Journal of Cell Biology 151, 709–718.

768 47. Taschner, M., Bhogaraju, S., and Lorentzen, E. (2012). Architecture and function of IFT complex  
769 proteins in ciliogenesis. Differentiation 83, S12–S22.

770 48. Eisa, N.H., Jilani, Y., Kainth, K., Redd, P., Lu, S., Bougrine, O., Abdul Sater, H., Patwardhan, C.A.,  
771 Shull, A., Shi, H., et al. (2019). The co-chaperone UNC45A is essential for the expression of mitotic  
772 kinase NEK7 and tumorigenesis. Journal of Biological Chemistry 294, 5246–5260.

773 49. Mooneyham, A., Iizuka, Y., Yang, Q., Coombes, C., McClellan, M., Shridhar, V., Emmings, E., Shetty,  
774 M., Chen, L., Ai, T., et al. (2019). UNC-45A Is a Novel Microtubule-Associated Protein and Regulator of  
775 Paclitaxel Sensitivity in Ovarian Cancer Cells. Molecular Cancer Research 17, 370–383.

776 50. Nicholls, P., Bujalowski, P.J., Epstein, H.F., Boehning, D.F., Barral, J.M., and Oberhauser, A.F. (2014).  
777 Chaperone-mediated reversible inhibition of the sarcomeric myosin power stroke. FEBS Letters 588,  
778 3977–3981.

779 51. Kobayashi, D., and Takeda, H. (2012). Ciliary motility: the components and cytoplasmic  
780 preassembly mechanisms of the axonemal dyneins. Differentiation 83, S23–29.

781 52. Rosenbaum, J.L., and Witman, G.B. (2002). Intraflagellar transport. Nat. Rev. Mol. Cell Biol. 3, 813–  
782 825.

783 53. Assimon, V.A., Southworth, D.R., and Gestwicki, J.E. (2015). Specific binding of tetratricopeptide  
784 repeat (TPR) proteins to heat shock protein 70 (Hsp70) and heat shock protein 90 (Hsp90) is regulated  
785 by affinity and phosphorylation. *Biochemistry* 54, 7120–7131.

786 54. Pal, M., Morgan, M., Phelps, S.E.L., Roe, S.M., Parry-Morris, S., Downs, J.A., Polier, S., Pearl, L.H.,  
787 and Prodromou, C. (2014). Structural Basis for Phosphorylation-Dependent Recruitment of Tel2 to  
788 Hsp90 by Pih1. *Structure* 22, 805–818.

789 55. X-linked primary ciliary dyskinesia due to mutations in the cytoplasmic axonemal dynein assembly  
790 factor PIH1D3.

791 56. Cho, K.J., Noh, S.H., Han, S.M., Choi, W.-I., Kim, H.-Y., Yu, S., Lee, J.S., Rim, J.H., Lee, M.G.,  
792 Hildebrandt, F., et al. (2018). ZMYND10 stabilizes intermediate chain proteins in the cytoplasmic pre-  
793 assembly of dynein arms. *PLoS Genet* 14,.

794 57. Jaffe, K.M., Grimes, D.T., Schottenfeld-Roames, J., Werner, M.E., Ku, T., Kim, S.K., Pelliccia, J.L.,  
795 Morante, N.F.C., Mitchell, B.J., and Burdine, R.D. (2016). c21orf59/kurly controls both cilia motility and  
796 polarization. *Cell Rep* 14, 1841–1849.

797 58. Diggle, C.P., Moore, D.J., Mali, G., zur Lage, P., Ait-Lounis, A., Schmidts, M., Shoemark, A., Garcia  
798 Munoz, A., Halachev, M.R., Gautier, P., et al. (2014). HEATR2 Plays a Conserved Role in Assembly of the  
799 Ciliary Motile Apparatus. *PLoS Genet* 10,.

800 59. Wang, G., Guo, Y., Zhou, T., Shi, X., Yu, J., Yang, Y., Wu, Y., Wang, J., Liu, M., Chen, X., et al. (2013).  
801 In-depth proteomic analysis of the human sperm reveals complex protein compositions. *Journal of*  
802 *Proteomics* 79, 114–122.

803 60. Amaral, A., Castillo, J., Estanyol, J.M., Ballescà, J.L., Ramalho-Santos, J., and Oliva, R. (2013). Human  
804 sperm tail proteome suggests new endogenous metabolic pathways. *Mol. Cell Proteomics* 12, 330–  
805 342.

806 61. Vandenbrouck, Y., Lane, L., Carapito, C., Duek, P., Rondel, K., Bruley, C., Macron, C., Gonzalez de  
807 Peredo, A., Couté, Y., Chaoui, K., et al. (2016). Looking for Missing Proteins in the Proteome of Human  
808 Spermatozoa: An Update. *Journal of Proteome Research* 15, 3998–4019.

- 809 62. Desai, P.B., Dean, A.B., and Mitchell, D.R. (2018). 4 - Cytoplasmic preassembly and trafficking of  
810 axonemal dyneins. In *Dyneins (Second Edition)*, S.M. King, ed. (Academic Press), pp. 140–161.
- 811 63. Auger, J., Jouannet, P., and Eustache, F. (2016). Another look at human sperm morphology. *Human*  
812 *Reproduction* *31*, 10–23.
- 813

814 **FIGURE LEGENDS**

815 **Figure 1. Ciliary and flagellar ultrastructural defects in PCD-affected individuals with *TTC12***  
816 **mutations**

817 Electromicrographs of cross-sections of ciliary axonemes (upper panel) from a control individual and  
818 individuals DCP153, 18GM00157, and DCP1606, compared to cross-sections of sperm flagellar  
819 axonemes (lower panel) from a control individual and from the infertile PCD-affected individuals  
820 DCP153 and DCP791. In each individual, the ciliary section shows an abnormal configuration with  
821 missing IDAs associated with a mild axonemal disorganization in individuals 18GM00157 and DCP1606,  
822 but with a clear presence of ODAs. The flagellar sections show a lack of both IDAs and ODAs. Black  
823 scale bars represent 0.1µm. NR: not relevant; NA: not available; IDAs: inner dynein arms; ODAs: outer  
824 dynein arms.

825

826 **Figure 2. *TTC12* mutations and their putative impact at the protein level in individuals with PCD**

827 The mutations are shown within the exonic organization of the human *TTC12* cDNA (top) and a  
828 domain-organization model of the corresponding protein (bottom) according to SMART webtool and  
829 CDD NCBI database. TPR: tetratricopeptide repeat; ARM: armadillo repeat. The light green box  
830 represents a degenerated ARM domain as opposed to the two dark green boxes that correspond to  
831 typical ARM domains.

832

833 **Figure 3. *TTC12* loss-of-function mutations cause defective single-headed inner dynein arm assembly**  
834 **in respiratory cilia**

835 **A)** Protein lysates extracted from AECs of a control individual and individuals 18GM00157, DCP1606  
836 and DCP153 were resolved by SDS-PAGE and analyzed by immunoblotting with an anti-*TTC12*  
837 antibody. The expression of *TTC12* is virtually absent or dramatically reduced in PCD-affected  
838 individuals. DNAJB13, a component of radial spokes, was used as positive control.

839 **B)** Immunofluorescence microscopy analysis of IDA markers in respiratory epithelial cells from a  
840 control and individuals 18GM00157, DCP1606 and DCP153 homozygous for *TTC12* mutations. Cells  
841 were double-labeled with an anti-acetylated  $\alpha$ -tubulin antibody (red), a marker of ciliary axonemes,  
842 and anti-DNAH6, anti-DNAH12 or anti-DNALI1 antibodies as markers of IDAs (green). Nuclear staining  
843 was performed with DAPI (blue). In affected individuals, DNAH12 is completely absent in the cilia but  
844 seems to accumulate at the subapical part of the cytoplasm. By contrast, DNALI1 and DNAH6 appear  
845 to be strongly reduced, but partially present at the proximal part of cilia. (DNAH2 and DNAH10, two  
846 markers of the double-headed IDA-I1 were shown to be normally expressed in the individuals, see  
847 Figure S7). Scale bars, 5  $\mu$ m.

848 IDA: inner dynein arm.

849

850 **Figure 4. *TTC12* mutations impact the assembly of both ODAs and IDAs in spermatozoa**

851 **A)** Immunofluorescence microscopy analysis of ODA and IDA markers in spermatozoa from a control  
852 and the infertile individual DCP153 carrying biallelic *TTC12* mutations. Cells were double-labeled with a  
853 marker of ciliary axonemes, anti- $\alpha$ -tubulin antibody (red), together with anti-DNAH8, anti-DNAH17 or  
854 anti-DNAI1 antibodies as markers of ODAs (green), and anti-DNAH3, anti-DNAH12 or anti-DNALI1  
855 antibodies as markers of IDAs (green). Nuclear staining was performed with DAPI (blue). In individuals  
856 DCP153, DNAH8, DNAH17, DNAI1 and DNAH3 are absent along the flagellar axoneme. By contrast,  
857 DNAH12 remains exclusively present in the proximal part of flagella, and DNALI1 appears to be present  
858 but reduced along the axoneme. Scale bars, 5  $\mu$ m.

859 **B)** Spermatozoa protein lysates of a control individual and individual DCP153 were resolved by SDS-  
860 PAGE and analyzed by immunoblotting with an anti-TTC12 antibody, showing the absence of TTC12  
861 expression in the individual. Very low amounts of TTC12 were detected in spermatozoa from the  
862 infertile individual DCP153. DNAJB13, a component of radial spokes, was used as positive control.

863 **C)** Spermatozoa protein lysates of a control individual and individual DCP153 were resolved by SDS-  
864 PAGE and analyzed by immunoblotting with an anti-DNALI1 antibody, showing the reduced amounts  
865 of DNALI1 in flagella from the affected individual. Actin was used as positive loading control.

866 ODA: outer dynein arm; IDA: inner dynein arm.

867

868 **Figure 5. Knockdown of *TTC12a* affects the swimming velocity of paramecia**

869 **A)** Z projection of track recording paramecia swimming under a dark-field microscope using a 10X  
870 objective after 24h or 48h of RNAi treatment. At 24h of silencing, swimming behaviour was affected in  
871 *TTC12a-* and *TTC12a+b-* silenced cells, while the silencing of *TTC12b* did not show any swimming  
872 defect. At 48h *TTC12a* and *TTC12a+b*-silenced cells did not swim anymore and died at 72hrs.

873 **B)** Analysis of the swimming velocity of *TTC12a*, *TTC12b* and *TTC12a+b* KD cells as well as control  
874 paramecia (i.e. empty vector silenced paramecia). Note that *TTC12b*-depleted cells swam slightly faster  
875 (725mm/sec) than control cells (EV, 665 mm/sec). The swimming velocity of *TTC12a* (317 mm/sec) and  
876 *TTC12a+b* (282 mm/sec) KD cells was reduced by 50% of that of control cells at 24h. Data are  
877 represented as the mean  $\pm$  SEM. Statistical analyses were performed with GraphPad Prism v5 software  
878 using two-tailed unpaired *t*-tests, \*\*\**p* < 0.001, \*\**p* < 0.01, (n=69-88 per experiment).

879 **C)** Z projection of track recording paramecia swimming under a dark-field microscope using a 10X  
880 objective. Transformed clones by *TTC12a* resistant-RNAi version (2c and 6c) as well as non-  
881 transformed paramecia were grown 36h in empty vector- or *TTC12a*-silencing media. *TTC12a*-depleted  
882 cells barely swam as shown previously, while cells expressing *TTC12a* resistant-RNAi version swam  
883 again similarly as control cells. This indicates that *TTC12a*-depleted phenotypes are rescued by *TTC12a*  
884 resistant-RNAi version.

885 **D)** Analysis of the swimming velocity of transformed and non-transformed cells grown in empty vector  
886 or *TTC12a*-silencing media. As expected, *TTC12a* silencing in non-transformed cells reduced  
887 dramatically the swimming velocity (52 mm/sec). However, the expression of the *TTC12* resistant-RNAi  
888 version rescues this phenotype (88% of complementation). Note that the swimming velocity of

889 transformed cells 2c (653 mm/sec) was similar as non-transformed paramecia (612 mm/sec), while  
890 transformed cells 6c swam slower (458 mm/sec). Data are represented as the mean  $\pm$  SEM. Statistical  
891 analyses were performed with GrahPad Prism v5 software using two-tailed unpaired *t*-tests,  
892 \*\*\* $p < 0.001$ , \*\* $p < 0.01$ , NS  $p > 0.1$  (n=26-48 per experiment).

893 **E)** Western blot analysis on total protein extract of transformed cells 2c and 6c showing that both  
894 clones express TTC12a-GFP.

895 EV: empty vector, KD: knockdown.

896

897 **Figure 6. Knockdown of *TTC12a+b* in paramecia leads to the loss of both ODAs and IDAs**

898 **A)** Depletion of *TTC12a+b* in *Paramecium* does not affect cilia number and length. *TTC12a+b* silenced  
899 paramecia were fixed and immunostained for cilia (anti-polyglutamylated tubulin antibodies) after 48h  
900 of RNAi. Scale bar, 20  $\mu$ m.

901 **B)** Upper panel: Electromicrographs of cross-sections of cilia from *TTC12a+b* KD paramecia. Control  
902 cilia show the normal distribution of both ODAs and IDAs. By contrast, *TTC12a+b* KD cilia show a partial  
903 or total lack of ODAs and IDAs. Scale bar, 200 nm.

904 Lower panel: Quantitative TEM analysis of IDAs and ODAs number on 140 cross-sections from a control  
905 and *TTC12a+b* co-depleted cells. ODAs and IDAs were normally distributed in 100% of cilia from  
906 control cells, and about 50% of the co-depleted *TTC12a+b* cells. This result has to be interpreted while  
907 taking into account that, in paramecia, half of cilia is renewed at each cell division. Therefore, after the  
908 first division, paramecia display half of normal cilia and half of *TTC12a+b*- silenced cilia. The former half  
909 (generated before silencing) did not display the phenotype while the new one did (generated after  
910 silencing).

911 ODA: outer dynein arm; IDA: inner dynein arm; KD: knockdown.

912

913 **Figure 7. *TTC12* is required for the assembly of single-headed inner dynein arms**



914 **A)** *TTC12* was invalidated in AEC cultures with *TTC12* CRISPR-Cas9 lentiviruses, and immunostained  
915 with an anti-acetylated  $\alpha$ -tubulin antibody (red), a marker of ciliary axonemes, and anti-DNAH6, anti-  
916 DNAH12 or anti-DNALI1 antibodies as markers of single-headed IDAs (green). Immunofluorescence  
917 analysis in ciliated cells clusters shows the partial invalidation of *TTC12* in culture with a loss of DNAH6,  
918 DNAH12 and DNALI1 in cells lacking *TTC12*. Scale bars, 25  $\mu$ m. DNAH6, DNAH12, and DNALI1 labeled  
919 areas were measured with ImageJ software and normalized against tubulin labeled area. The  
920 dynein/tubulin ratios obtained in *TTC12*-CRISPR transduced cells were then normalized to ratios  
921 obtained in EV-transduced cells. Values of those final ratios are indicated on the right of the  
922 histograms, and showed the decrease of dynein chain labeling signal compared to tubulin. Data are  
923 represented as the mean  $\pm$  SEM. Statistical analyses were performed with GrahPad Prism v5 software  
924 using two-tailed unpaired *t*-tests, \*\*\**p*<0.001 (n=3).

925 **B)** Immunofluorescence images of isolated ciliated cells lacking *TTC12* showing the complete loss of  
926 DNAH12 along the cilia and its accumulation in the subapical region of the cytoplasm, while DNAH6  
927 and DNALI1 expression appears strongly decreased but still present at the base of cilia. Nuclear  
928 staining was performed with DAPI (blue). Scale bar, 25  $\mu$ m.

929 **C)** Electromicrographs of cross-sections of cilia axonemes from a non-infected AEC culture and a  
930 *TTC12*-CRISPR-infected cell culture show an abnormal arrangement lacking IDAs in the *TTC12*-  
931 invalidated culture. Proportion in electromicrograph cross-sections of cilia harboring more than four  
932 IDAs, between two and four IDAs, and up to one IDA, were reported in a histogram comparing control  
933 cells to *TTC12*-invalidated cells. Scale bars, 5  $\mu$ m.

934 ODA: outer dynein arm; IDA: inner dynein arm; EV: empty vector.

935

936 **Figure 8. Dynein chains affected by the absence of *TTC12* and diagrammatic representation of the**  
937 **axonemal components impacted by *TTC12* loss-of-function mutations in respiratory cilia and sperm**  
938 **flagella**

939 **A)** Table summarizing the dynein chains studied by immunofluorescence in AECs of a control,  
940 individuals 18GM00157, DCP1606, DCP153, AEC cultures invalidated or not for *TTC12* by a CRISPR-cas9  
941 approach, as well as in spermatozoa from a control and individual DCP153. ODA labeling was  
942 performed with anti-DNAH5 and anti-DNAH9 antibodies in AECs, and anti-DNAH8 and anti-DNAH17  
943 antibodies in spermatozoa. Black check marks represent normal localization, minus signs represent an  
944 absence of protein, and black cross signs indicate mislocalization. NR: not relevant.

945 **B)** Schematic structure of a normal 96 nm-long axonemal unit. Each unit, which repeats along the  
946 microtubule doublets, consists of four ODAs represented in purple and IDAs shown in blue. As the  
947 exact composition of IDAs is virtually unknown in humans, the IDA representation is based on data  
948 from *Chlamydomonas* in which the seven IDA subspecies include six single-headed dynein arms (a, b, c,  
949 e, g, d) and one double-headed dynein arm (IDA-I1).

950 **C)** Phenotype of *TTC12*-deficient respiratory cilia versus *TTC12*-deficient sperm flagella. The proteins  
951 unaffected by the loss of *TTC12* are represented in full color and written in yellow and the proteins  
952 affected by the loss of *TTC12* are represented in white with red dotted line and written in red. The  
953 proteins found to be affected by *TTC12* mutations but for which the exact localization is unknown in  
954 humans, are represented in hatched red pattern and written in red. Proteins with lower but non-null  
955 expression are represented in hatched grey pattern and written in red. The proteins that could not be  
956 tested are represented and written in grey.

957 ODA: outer dynein arm; IDA: inner dynein arm; N-DRC: nexin-dynein regulatory complex; MIA:  
958 modifier of inner arms; IC/LC: intermediate chain/light chain, RS: radial spoke; MT: microtubules.

959

960 **Movie S1.** Representative movie showing immotile cilia of individual 18GM00157.

961 **Movie S2.** Representative movie beating cilia of individual 18GM00157.

962 **Movie S3.** Representative movie showing immotile cilia of individual DCP1606.

963 **Movie S4.** Representative movie showing beating cilia of individual DCP1606.

964 **Movie S5.** Representative movie showing showing immotile cilia of individual DCP153.

965 **Movie S6.** Representative movie showing beating cilia of individual DCP153.

966 **Movie S7.** Representative movie showing beating cilia of control individual.

967

## TABLES

Table 1: Phenotype of PCD-affected individuals with identified *TTC12* mutations

Individuals (Origin)	Known Consanguinity	Gender (Age at Diagnosis)	SI	Airway Disease		Fertility	Nasal NO (nL/min)	TEM defect (%)		Allele 1	Allele 2
				Lower	Upper			Cilia	Sperm		
<b>DCP791</b> (Turkey)	Yes	Male (24 years)	No	Minima	Sinusitis	Infertility	Low <sup>a</sup>	NA	IDAs+ ODAs (100%)	c.1614+3A>T p.?	c.1614+3A>T p.?
<b>18GM00157</b> (Morocco)	Yes	Female (50 years)	No	Asthma Bronchiectasis	Rhino- sinusitis	Not tested	37.6	IDAs (100%) Disorganization (22%)	NR	c.1678C>T p.Arg560*	c.1678C>T p.Arg560*
<b>DCP1606</b> (Tunisia)	Yes	Male (11 years)	No	NNRD Bronchiectasis Pneumopathies	Rhino- sinusitis Otitis	NR	146	IDAs (100%) Disorganization (24%)	NR	c.607del p.Ile203*	c.607del p.Ile203*
<b>DCP153</b> (Europe)	No	Male (33 years)	No	Bronchitis	Rhino- sinusitis	Infertility	186	IDAs (100%) Disorganization (2%)	IDAs+ODAs (100%)	c.1700T>G p.Met567Arg	c.1700T>G p.Met567Arg

SI: situs inversus; NNRD: neonatal respiratory distress; NR: not relevant; NO: nitric oxide; ppb: parts per billion; CBF: ciliary beat frequency; Hz: hertz; NA: not available; TEM: transmission electron microscopy; Spz:

spermatozoa; IDAs: inner dynein arms, ODAs: outer dynein arms. PCD nasal NO < 77 nL/min<sup>8</sup>.

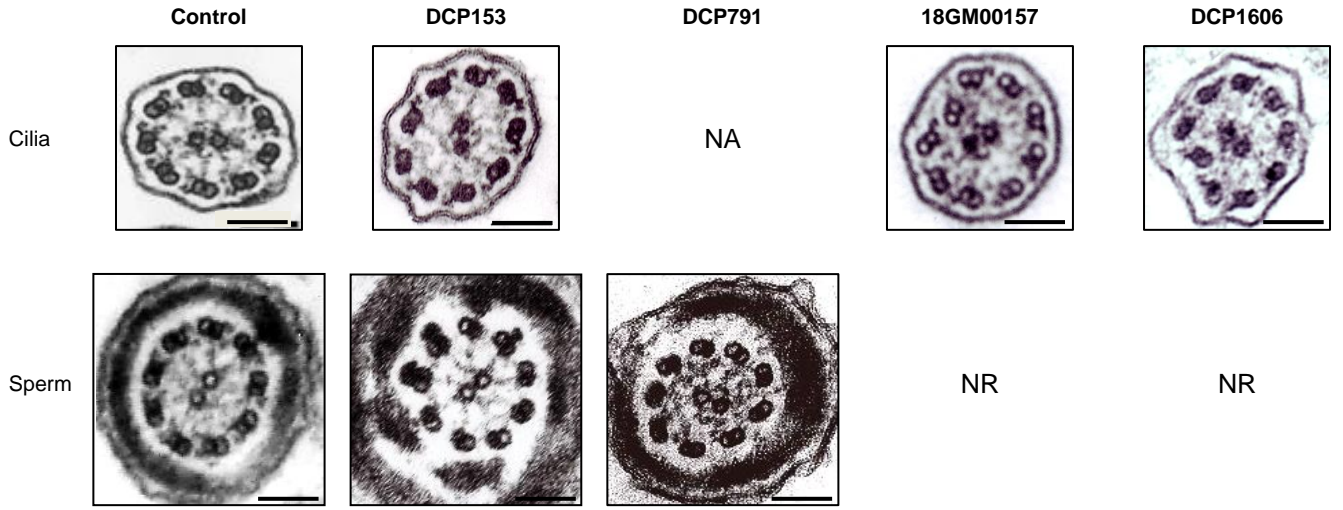
<sup>a</sup>exact value not available

Table 2. Semen characteristics of infertile individuals with identified *TTC12* mutations

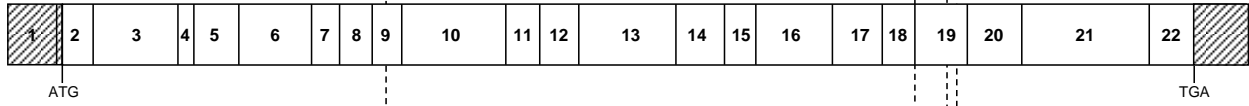
Individuals	pH	Volume (ml)	Sperm count (10 <sup>6</sup> /ml)	Total Motility (%)	Progressive Motility (%)	Vitality (%)	Typical forms (%)	Flagellum Defects				
								Absent	Short	Irregular Caliber	Coiled	Multiple
<b>DCP791</b>	ND	ND	21	<b>0</b>	<b>0</b>	75	36	7	0	0	10	0
<b>DCP153</b>	7.9	4.5	81	<b>0</b>	<b>0</b>	68	33	2	1	1	6	1
<b>Reference values</b> <sup>a</sup>	7.2	1.5	15	40	32	58	23	5	1	2	17	1

Values are expressed in percent, unless otherwise specified. ND: not determined.

<sup>a</sup> According to the World Health Organization (WHO) standards<sup>23</sup> and the distribution range of morphologically abnormal spermatozoa observed in fertile individuals<sup>63</sup>; in bold characters: abnormal values



**TTC12**  
cDNA  
NM\_017868.4



**DCP1606**  
c.607del  
p.Ile203\*

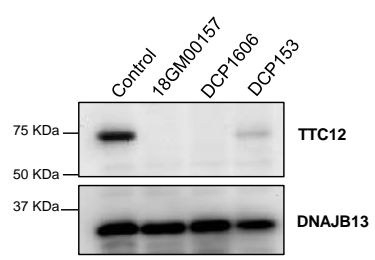
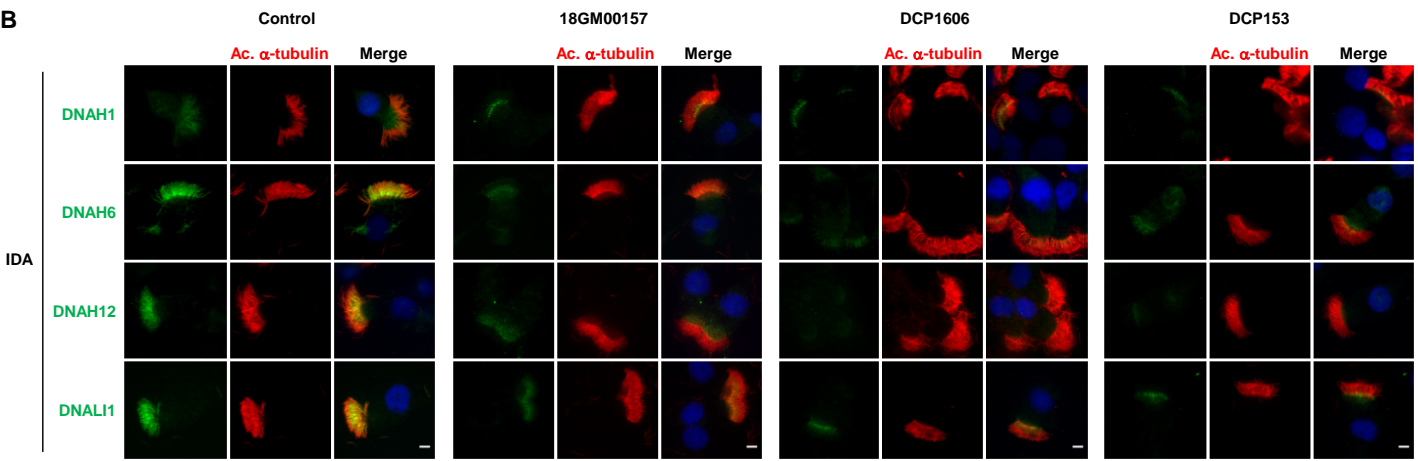
**DCP791**  
c.1614+3A>T  
p.?

**18GM00157**  
c.1678C>T  
p.Arg560\*

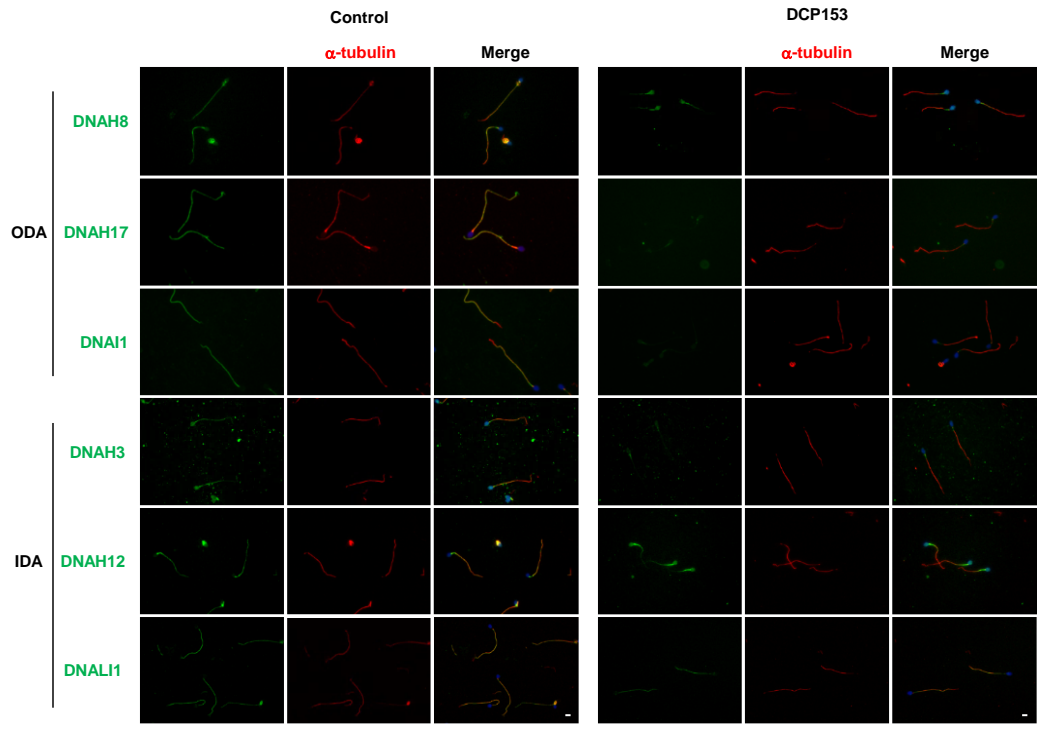
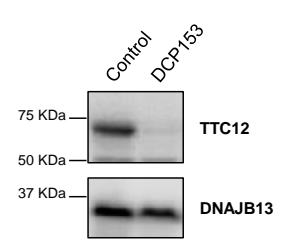
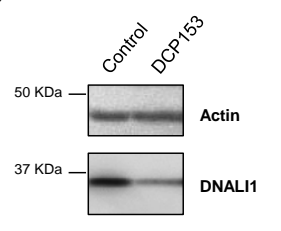
**DCP153**  
c.1700T>G  
p.Met567Arg

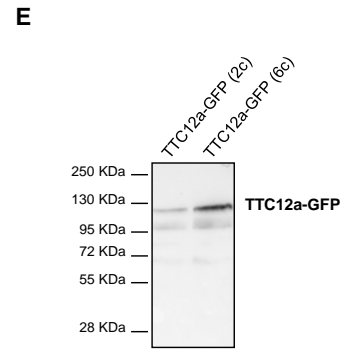
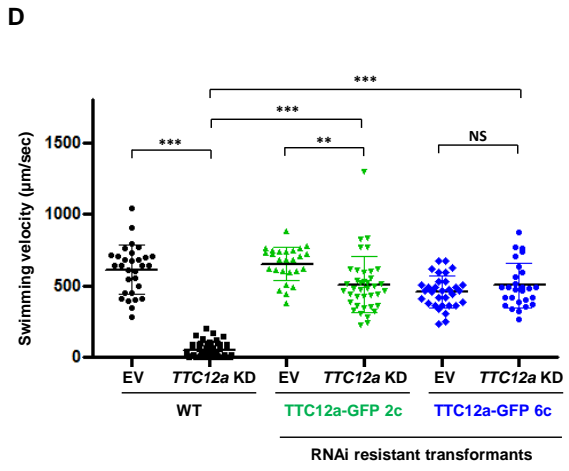
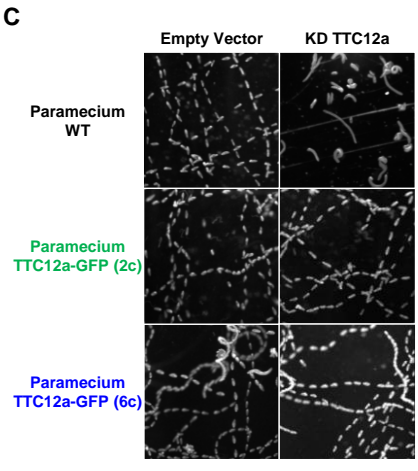
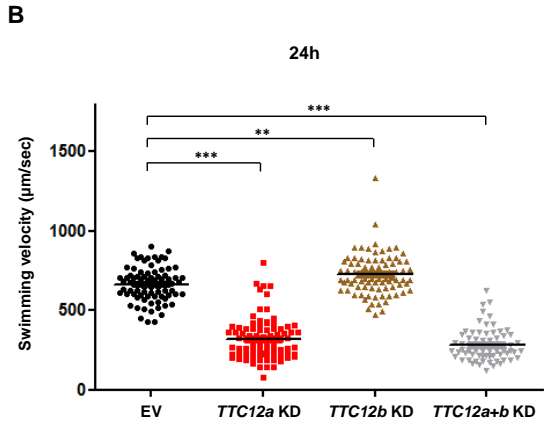
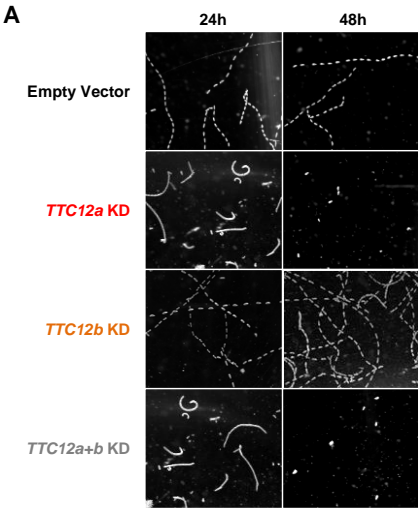
**TTC12**  
*Homo sapiens*

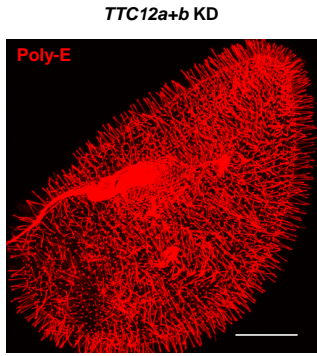
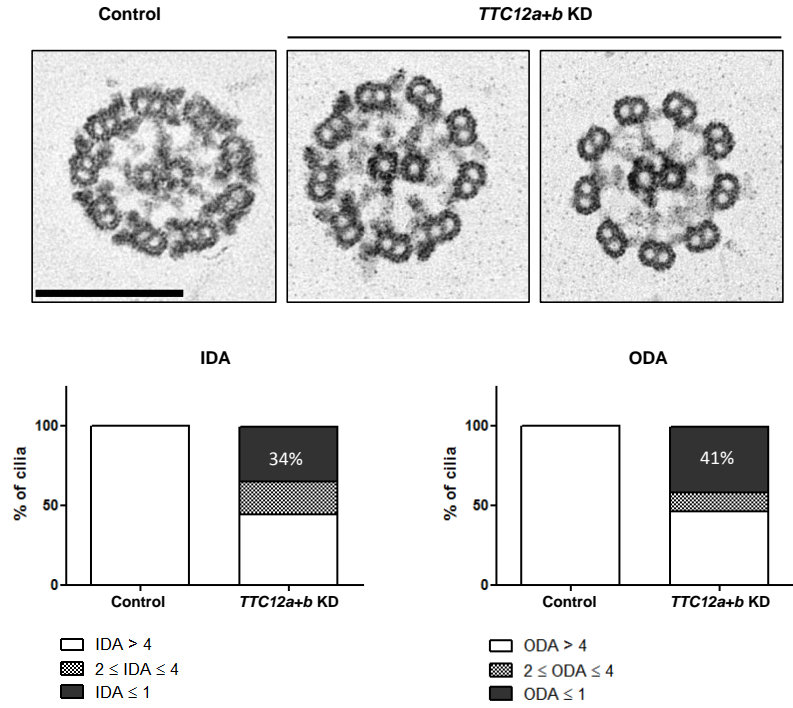


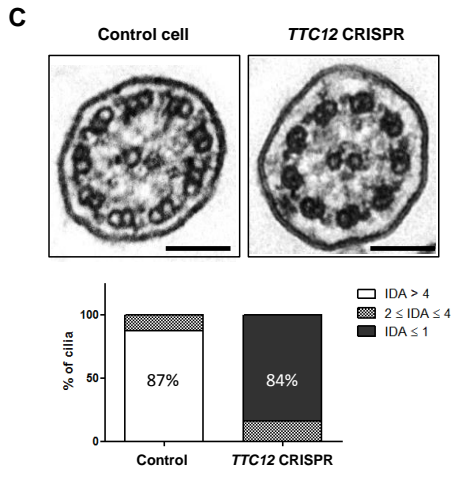
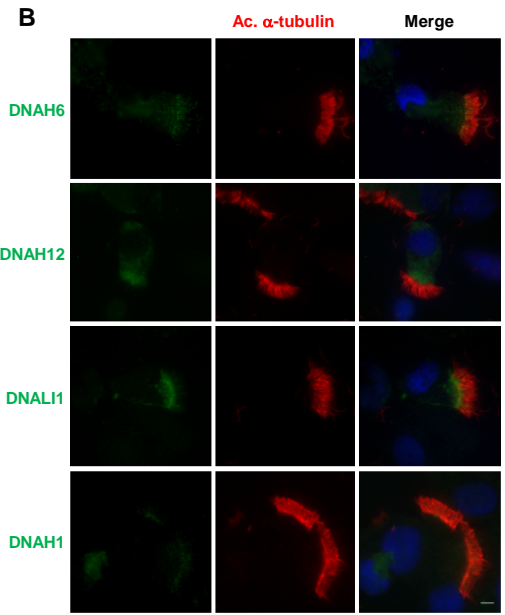
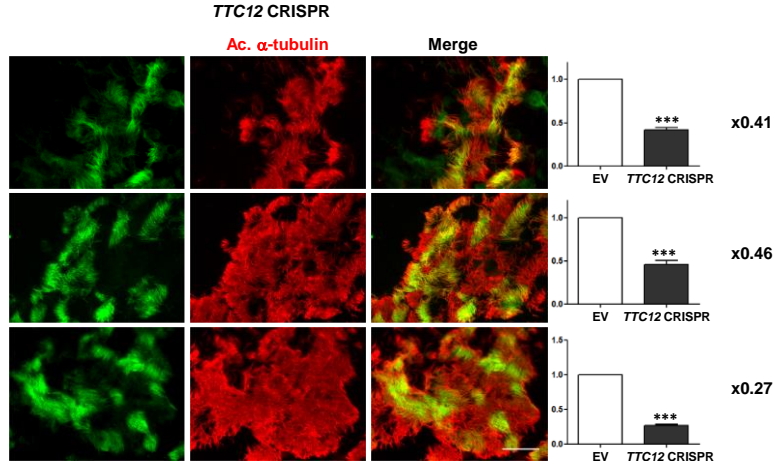
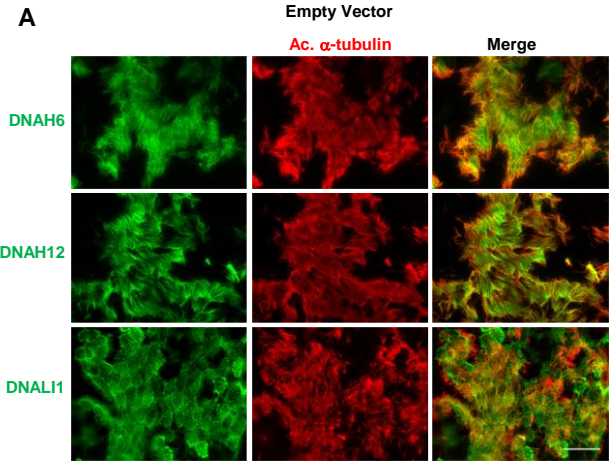
**A****B**



**A****B****C**



**A****B**



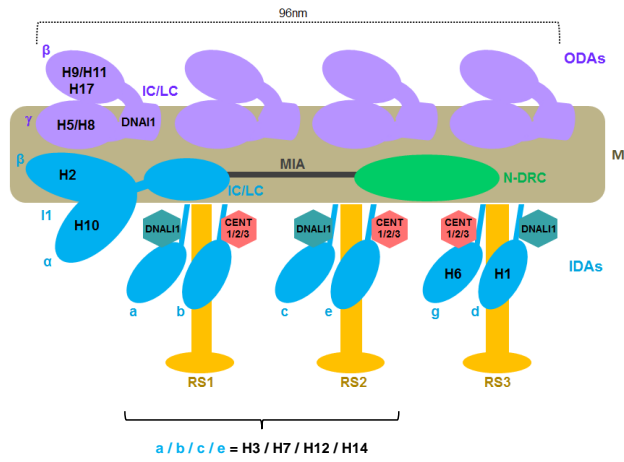
**A**

	Respiratory cilia						Sperm flagella	
	Control	1809100357	Dcp1-696	Dcp123	Empty Vector	TTC12 CRISPR	Control	Dcp123
ODA	DNAH5/H8*	✓	✓	✓	✓	✓	✓	✗
	DNAH9/H17*	✓	✓	✓	✓	✓	✓	✗
	DNAH11	✓	✓	✓	✓	✓	-	NR
	DNAI1	✓	✓	✓	✓	✓	✓	✗
IDA	DNAH2	✓	✓	✓	✓	✓	✓	✓
	DNAH10	✓	✓	✓	✓	✓	✓	✓
	DNAH1	✓	✗	✗	✗	✓	✗	✓
	DNAH3	-	NR	NR	NR	NR	NR	✗
	DNAH6	✓	✗	✗	✗	✓	✗	✓
	DNAH12	✓	✗	✗	✗	✓	✗	✗
	DNAL1	✓	✗	✗	✗	✓	✗	✗
		✓	✗	✗	✗	✓	✗	✗

✓: present; ✗: mislocalized; -: absent; NR: not relevant

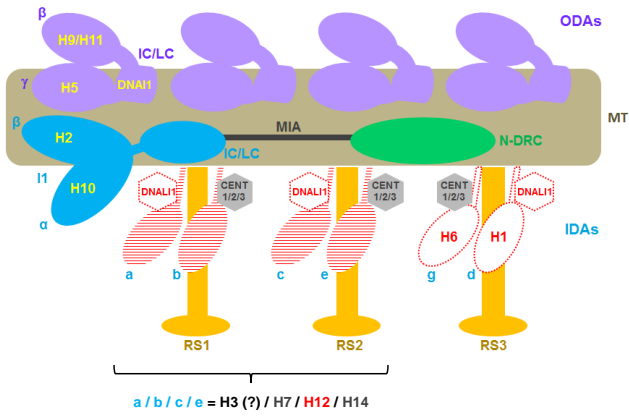
\* Respiratory cilia: DNAH5 and DNAH9; Sperm flagella: DNAH8 and DNAH17

**B**



**C**

Respiratory cilia



Sperm flagella

